Published in "Plant Physiology 173(1): 788–800, 2017"
which should be cited to refer to this work.

SHADE AVOIDANCE 4 Is Required for Proper Auxin Distribution in the Hypocotyl[1]

Yanhua Ge, Fenglian Yan, Melina Zourelidou, Meiling Wang, Karin Ljung, Astrid Fastner, Ulrich Z. Hammes, Martin Di Donato, Markus Geisler, Claus Schwechheimer, and Yi Tao*

School of Life Sciences, Xiamen Plant Genetics Key Laboratory (Y.G., F.Y., M.W., Y.T.), and State Key Laboratory of Cellular Stress Biology (Y.G., Y.T.), Xiamen University, Xiamen 361102, China; Department of Plant Systems Biology, Technische Universität München, Freising 85354, Germany (M.Z., C.S.); Umeå Plant Science Centre, Department of Forest Genetics and Plant Physiology, Swedish University of Agricultural Sciences, SE-901 83 Umeå, Sweden (K.L.); Department of Cell Biology and Plant Biochemistry, Universität Regensburg, Regensburg 93047, Germany (A.F., U.Z.H.); and Department of Biology-Plant Biology, University of Fribourg, CH-1700 Fribourg, Switzerland (M.D.D., M.G.)

ORCID IDs: 0000-0003-2901-189X (K.L.); 0000-0002-5642-2523 (M.D.D.); 0000-0002-6641-5810 (M.G.); 0000-0002-4438-606X (C.S.); 0000-0002-7460-7927 (Y.T.).

The phytohormone auxin is involved in virtually every aspect of plant growth and development. Through polar auxin transport, auxin gradients can be established, which then direct plant differentiation and growth. Shade avoidance responses are well-known processes that require polar auxin transport. In this study, we have identified a mutant, *shade avoidance 4* (*sav4*), defective in shade-induced hypocotyl elongation and basipetal auxin transport. *SAV4* encodes an unknown protein with armadillo repeat- and tetratricopeptide repeat-like domains known to provide protein-protein interaction surfaces. C terminally yellow fluorescent protein-tagged SAV4 localizes to both the plasma membrane and the nucleus. Membrane-localized SAV4 displays a polar association with the shootward plasma membrane domain in hypocotyl and root cells, which appears to be necessary for its function in hypocotyl elongation. Cotransfection of SAV4 and ATP-binding cassette B1 (ABCB1) auxin transporter in tobacco (*Nicotiana benthamiana*) revealed that SAV4 blocks ABCB1-mediated auxin efflux. We thus propose that polarly localized SAV4 acts to inhibit ABCB-mediated auxin efflux toward shoots and facilitates the establishment of proper auxin gradients.

The phytohormone auxin controls almost every aspect of plant growth and development, ranging from embryogenesis to organogenesis and tropic responses (Vieten et al., 2007; Petrasek and Friml, 2009; Vanneste and Friml, 2009). Formation of an auxin gradient within the plant is determined by both local auxin biosynthesis and conjugation/degradation as well as directional cell-to-cell transport system (Vieten et al., 2007; Mashiguchi et al., 2011; Pencík et al., 2013; Zheng et al., 2016). This system, called polar auxin transport, is composed of auxin transport proteins, including the AUXIN RESISTANT1/LIKE-AUXIN RESISTANT1 family of influx carriers (Péret et al., 2012; Swarup and Péret, 2012), the PIN-FORMED (PIN), and some members of the ATP-binding cassette B type/PHOSPHOGLYCOPROTEIN (ABCB/PGP) families of efflux facilitators (Müller et al., 1998; Friml et al., 2002; Geisler et al., 2005; Blakeslee et al., 2007). Among them, polarly localized PINs play a major role in determining the directionality of auxin flow, thus leading to the accumulation of auxin in some tissues and organs (Petrásek et al., 2006; Wisniewska et al., 2006). This auxin gradient plays an important role in plant development and enables plants to adjust their development, architecture and growth in response to changes in their local environment.

Under vegetative shade, shade-intolerant species, such as Arabidopsis (*Arabidopsis thaliana*), respond by a series of morphological changes, including stem and petiole elongation, leaf hyponasty and retarded leaf

[1] Early stages of these studies were performed in the laboratory of Joanne Chory at The Salk Institute for Biological Studies and were supported by the Howard Hughes Medical Institute and U.S. National Institutes of Health Grant 5R01GM52413 to Joanne Chory. This work was supported by grants from the National Natural Science Foundation of China (grant nos. 31171162 and 31271298 to Y.T.), the Fundamental Research Funds for the Central Universities of China (grant no. 2012121041 to Y.T.), and the 111 Project B12001. Funding for open access provided by the National Natural Science Foundation of China. This work was also supported by the Swedish Governmental Agency for Innovation Systems and the Swedish Research Council to K.L. and the Swiss National Funds to M.G. Y.G. was recipient of a travel grant from the SFB924 (Deutsche Forschungsgemeinschaft) awarded to C.S. C.S. is supported by a grant from the Deutsche Forschungsgemeinschaft SCHW 751/12-1.

* Address correspondence to yitao@xmu.edu.cn.

The author responsible for distribution of materials integral to the findings presented in this article in accordance with the policy described in the Instructions for Authors (www.plantphysiol.org) is: Yi Tao (yitao@xmu.edu.cn).

Y.G., C.S., and Y.T. designed the research; Y.G., F.Y., M.Z., M.W., K.L., A.F., and M.D.D. performed the research; Y.G., U.Z.H., M.G., C.S., and Y.T. discussed the data; Y.G., M.G., C.S., and Y.T. wrote the article with contributions from the other authors.

development, which are collectively referred to as the shade avoidance syndrome (SAS; Franklin and Whitelam, 2005; Casal, 2013; Hersch et al., 2014). Reduction in the red:far-red light (R:FR) ratio is the most efficient signal to induce the SAS and can be used to mimic canopy shade in experimental settings (Cole et al., 2011). The rapid elongation of stems and petioles are the most prominent SAS responses, through which the shaded plants attempt to outgrow their competitors and secure the photosynthetic organs to light capture. Accumulating evidences point to auxin as a key regulator of the SAS, as mutants defective in auxin biosynthesis (*Trp aminotransferase of Arabidopsis/sav3* [*taa1/sav3*]), transport (*pin3*), or signaling (*tir1*) are defective in shade-induced hypocotyl elongation (Tao et al., 2008; Keuskamp et al., 2010). It was proposed that low R:FR signal induces auxin biosynthesis in cotyledons and emerging young leaves, which is then transported to the hypocotyls to promote hypocotyl elongation (Tao et al., 2008). Shade will induce the relocation of PIN3 from the basal end to the lateral side of the endodermal cells, thus redirecting auxin toward the epidermal cell layers and promoting cell elongation (Morelli and Ruberti, 2000; Keuskamp et al., 2010). Within the hypocotyl, the epidermis is most efficient in driving or restricting hypocotyl growth (Savaldi-Goldstein et al., 2007; Procko et al., 2016; Zheng et al., 2016). PIN3 is a key auxin transporter mediating low R:FR-induced hypocotyl elongation, but it remains poorly understood how PIN3 is repolarized in response to the low R:FR signal in shaded plants (Keuskamp et al., 2010).

Previous studies have revealed that regulation of auxin transporters occurs at multiple levels. First, phosphorylation was proposed to modulate the polar targeting or transporter activity of PIN proteins (Friml et al., 2004; Zourelidou et al., 2014). The AGCVIII kinases PINOID (PID), WAG1, and WAG2 could instruct recruitment of PINs into the apical recycling pathway by phosphorylating serines in three conserved TPRXS (N/S) motifs within the PINs' cytoplasmic loop (Dhonukshe et al., 2010; Huang et al., 2010). Overexpression of PID, which presumably enhanced PIN phosphorylation, causes a rootward-to-shootward PIN polarity shift, leading to auxin depletion from the root meristem and resulting in root meristem collapse (Friml et al., 2004). On the contrary, phenotypes of *pid* loss-of-function mutant may be explained by a shootward-to-rootward shift in PIN polarity, causing developmental defects in embryos as well as impaired shoot and inflorescence differentiation (Benjamins et al., 2001; Friml et al., 2004).

Besides the proposed role of PID in controlling PIN polarity, PID and the related WAG2 also activate PIN-mediated auxin transport when tested in heterologous systems (Zourelidou et al., 2014). This activity was uncovered during studies of D6 PROTEIN KINASEs (D6PKs), which belong to a subgroup of AGCVIII kinases. D6PKs can directly phosphorylate PINs and increase their auxin transport activity (Zourelidou et al., 2009, 2014; Willige et al., 2013). Consequently, *d6pk* mutants showed defects in auxin transport when examined in shoots and hypocotyls and defects in hypocotyl gravitropic and phototropic bending (Willige et al., 2013; Barbosa et al., 2014; Zourelidou et al., 2014). Interestingly, D6PKs and PID have different phosphosite preferences for an overlapping set of PIN phosphosites. These results indicate that phosphorylation of PINs is regulated by multiple kinases, and the phosphorylation of a specific site(s) may affect PIN polarity and/or activity (Zourelidou et al., 2014). Recent results suggested that ABCB1 and ABCB19 are phosphorylated by PID and PHOTOTROPIN1 (PHOT1), respectively, which directly influence their auxin-efflux transporter activity (Christie et al., 2011; Henrichs et al., 2012).

Interactions between transporters represent an additional layer of auxin transport regulation. Blakeslee et al. (2007) reported that ABCB1/PGP1 and ABCB19/PGP19 physically interact with PINs, and these interactions appear to enhance the auxin transport activity and substrate/inhibitor specificities in a heterologous yeast system. *abcb19* and *abcb1 abcb19* mutants exhibited significantly reduced rootward auxin flow in both the hypocotyls and inflorescence stems (Noh et al., 2001). Further studies revealed that ABCB19 stabilizes PIN1 at the plasma membrane so as to coordinately regulate auxin efflux (Titapiwatanakun et al., 2009). Thus, the formation of an auxin gradient is achieved through regulations of the subcellular localization and activity of auxin transporters by means of protein modification and/or interactions with other proteins.

In this study, we identify and characterize SAV4 as a novel regulator of shade avoidance. We show that mutation in *SAV4* leads to defects in shade-induced hypocotyl elongation and basipetal auxin transport. Cotransfection of SAV4 and ABCB1 in tobacco (*Nicotiana benthamiana*) blocks ABCB1-mediated auxin efflux, confirming its role in modulating auxin transport. Membrane-localized SAV4 displays a strong association with the shootward plasma membrane domain in hypocotyl and root cells, which appears to be necessary for its function in the hypocotyl elongation. We propose that polarly localized SAV4 may inhibit shootward auxin flow by inhibiting ABCB1-mediated auxin efflux and thus maintain the net auxin flow toward roots.

RESULTS

Identification and Phenotypic Characterization of the *sav4* Mutant

In a forward genetic screen, we identified *shade avoidance* (*sav*) mutants that were wild-type-like in continuous white light (Wc) but had shorter hypocotyls than the wild type in simulated shade (shade; R:FR ratio around 0.7; Tao et al., 2008). Hypocotyls of *sav4* were significantly shorter than those of the wild type in shade but were only slightly shorter than the wild type in dark (Fig. 1, A–C). This suggested a specific role of *SAV4* in shade-induced hypocotyl elongation.

Several phenotypic changes are associated with the shade avoidance responses, including petiole elongation,

lamina growth reduction, and increased leaf hyponasty (Franklin and Whitelam, 2005). We found that *sav4* mutants had shorter petiole and larger lamina size compared with the wild type under both Wc and shade (Supplemental Fig. S1, A and B). However, shade-induced leaf hyponasty was not affected in *sav4*, which was measured as the angle between the cotyledon-petiole and an artificial horizontal line drawn perpendicular to the hypocotyl (Supplemental Fig. S1C). We thus conclude that *SAV4* participates in some, but not all, shade avoidance responses.

Shade signal is perceived by photoreceptors such as phytochromes and cryptochromes, which then initiate a complex signaling cascade that modulates the architecture of plants to an ever-changing environment (Franklin and Whitelam, 2005; Casal, 2013). To determine if *SAV4* was required for light perception by a specific photoreceptor, we analyzed responses of *sav4* to monochromatic light (red, far-red, and blue light). Our results revealed that *sav4* was not defective in de-etiolation induced by the monochromatic light (Supplemental Fig. S1, D–F), indicating that *sav4* is normal in light perception.

In summary, *SAV4* is specifically required for shade-induced hypocotyl elongation, whereas its defects in petiole elongation and lamina growth seem to be independent of light conditions.

Map-Based Cloning of *SAV4*

sav4 behaved as a single recessive mutation as an F2 backcrossed population displayed a close to 3:1 phenotypic segregation under shade (287 long and 92 short hypocotyls, fitting an expected 3:1 ratio: $\chi^2 = 0.744 < \chi^2_{0.05} = 3.84$, $df = 1$). Through map-based cloning, we mapped the mutation to a 25-kb region between markers T31P16 and F18D22 on chromosome 5 containing 11 annotated genes. Direct sequencing revealed a G to A mutation in *At5G10200* that converts Trp-218 of the 631 amino acid long protein to a stop codon (Fig. 2A). A complementation test was performed by introducing a 5-kb genomic DNA fragment of the wild-type *At5G10200* into the *sav4* mutant. The transgene complemented the short hypocotyl phenotype of *sav4* in shade (Fig. 2, B and C), demonstrating that the phenotype of *sav4* is due to the defective *At5G10200* (*SAV4*) gene.

SAV4 contains a putative ARM repeat- and a TPR-like domain, both of which are often involved in protein-protein interactions and the assembly of multiprotein complexes. Results from a distance-based neighbor-joining phylogenetic analysis revealed that SAV4 shares high homology with maize GRMZM2G020409 and GRMZM2G057184 as well as the rice Os05G34820 (Fig. 2D). However, nothing is known about the function of SAV4 and these apparent orthologs. There has been no report of a *sav4* loss-of-function mutant and no T-DNA insertion mutant is available for this gene. The SUBA3 program (http://suba.plantenergy.uwa.edu.au/) predicted that SAV4 would localize to the nucleus, while quantitative mass spectrometry data suggested a possible plasma membrane localization of SAV4 (Benschop et al., 2007). Nonetheless, there is no putative hydrophobic transmembrane domain identified in SAV4.

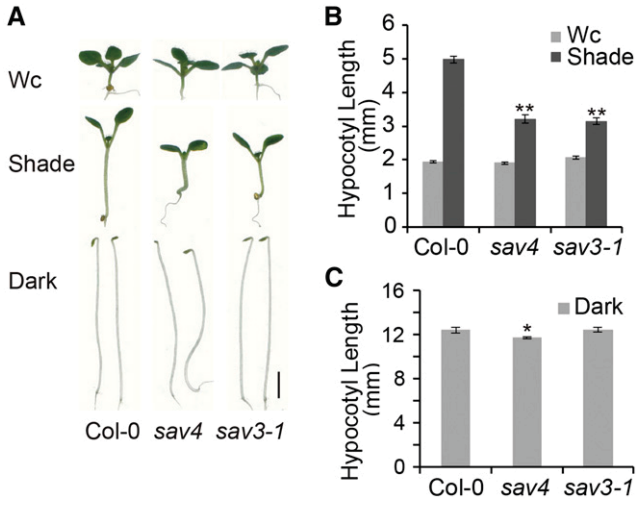

Figure 1. Hypocotyl phenotype of the *sav4* mutant. A, Hypocotyl phenotype of the wild-type and mutant seedlings under different light conditions. The wild-type Col-0, *sav4*, and *sav3-1* were grown in Wc for 6 d, and then transferred to shade or kept in Wc for another 3 d. Three-day-old etiolated seedlings of the respective genotype are shown at the bottom. B and C, Quantification of hypocotyl length in seedlings shown in A. Error bars represent the SEM ($n \geq 20$). Scale bar = 2 mm. Student's *t* test, compared with the wild-type Col-0: $^*P < 0.05$, $^{**}P < 0.01$.

Tissue-Specific Expression Patterns of *SAV4*

To investigate the expression pattern of *SAV4*, we generated *SAV4::SAV4-GUS* transgenic lines using the *SAV4* promoter fragment and the genomic *SAV4* fused in frame to the GUS reporter. The transgene complemented the *sav4* hypocotyl phenotype in shade, indicating that it is functional (Supplemental Fig. S2A). SAV4-GUS exhibited GUS activities throughout the seedling in both light and dark conditions. Strong expression was detected in the emerging leaf primordia and root apical meristems as well as in vascular tissues of the hypocotyls and leaf blades (Fig. 3, C and D). GUS signal was visible in both stele and the endodermis (Fig. 3E). *SAV4* was also expressed in the pistils, the stamens, and the vasculature of petals and sepals (Fig. 3, F–H). Taken together, *SAV4* was shown to be predominantly expressed in young organs, elongating tissues and the vasculatures.

In view of the shade avoidance phenotypes of *sav4*, we also investigated whether the transcript level of *SAV4* was altered in shade using quantitative real-time reverse transcriptase PCR (qRT-PCR). The results showed that *SAV4* transcript level is relatively stable in response to shade, suggesting that *SAV4* is not regulated at the transcriptional level during the shade avoidance response (Supplemental Fig. S2B).

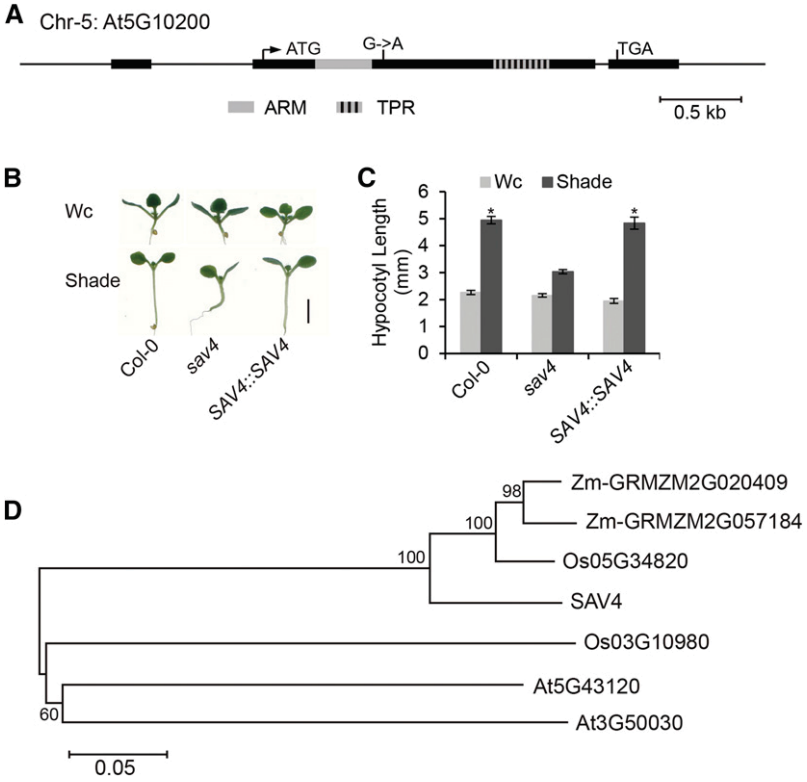

Figure 2. Cloning and genetic complementation of *sav4*. A, Schematic representation of the *At5G10200* genomic fragment used for the complementation experiment. The *sav4* mutant carries a G to A substitution, converting Trp-218 to a stop codon. Black boxes represent exons, and black lines represent introns or nontranscribed regions. B and C, Complementation of the short hypocotyl phenotype of *sav4* in shade by the wild-type genomic *SAV4* (*SAV4::SAV4*). Error bars represent the SEM ($n \geq 20$). Scale bar = 2 mm. Student's *t* test, compared with *sav4*: $^*P < 0.01$. D, Phylogenetic tree analysis of SAV4 protein. Values below branches indicate bootstrap values. Bar = 0.05 amino acid substitutions per site. At, *Arabidopsis thaliana*; Os, *Oryza sativa*; Zm, *Zea mays*.

SAV4 Exhibits a Dual Localization at the Plasma Membrane and the Nucleus

To further examine the subcellular localization of SAV4, *SAV4::SAV4-YFP* transgenic lines expressing a C-terminal yellow fluorescent protein (YFP)-fused SAV4 under the control of *SAV4* promoter were generated. Recombinant SAV4-YFP was able to rescue the hypocotyl phenotype of *sav4* in shade (Supplemental Fig. S2A). Interestingly, SAV4-YFP was detected at the plasma membrane as well as in the nucleus (Fig. 4, A–G). Membrane-localized SAV4 exhibited a polar localization in that it was predominately localized to the apical (shoot apical meristem-directed) side in most cell types examined (Fig. 4, A–D; Supplemental Fig. S3). To confirm the plasma membrane localization of SAV4-YFP, a plasmolysis experiment was performed using roots of *SAV4::SAV4-YFP*. We found that SAV4-YFP colocalizes with the plasma membrane marker FM4-64 in plasmolyzed cells, supporting that SAV4-YFP is indeed associated with the plasma membrane (Fig. 4, E and F). Nuclear localization of SAV4 was confirmed by colocalization with 4′,6-diamino-phenylindole (DAPI) in the nucleus (Fig. 4G). The subcellular localization of SAV4 suggests that it may be multifunctional. For example, it may influence gene expression in the nucleus and may affect auxin transport at the plasma membrane.

The dual localization of SAV4 prompted us to investigate whether specific regions of SAV4 define its

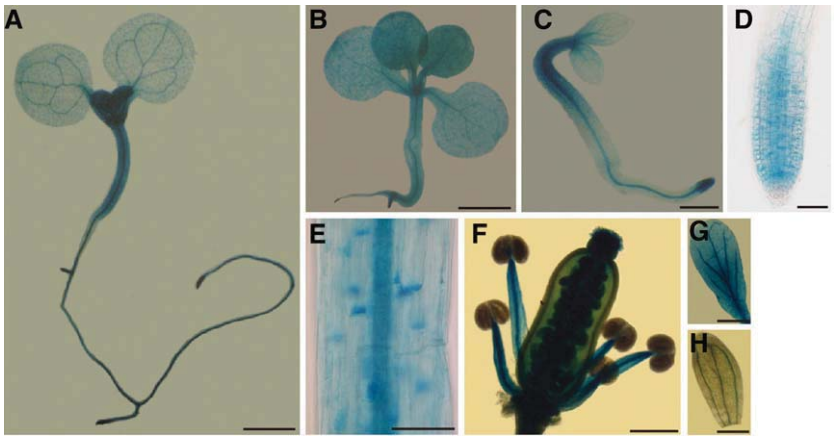

Figure 3. Expression pattern analysis of *SAV4*. GUS activity in the representative transgenic line carrying the *SAV4-GUS* reporter gene (*SAV4::SAV4-GUS*) in light-grown seedlings 6 DAG (A), light-grown seedlings at 10 DAG (B), dark-grown seedlings at 2 DAG (C), root tip (D), upper hypocotyl of 2-DAG dark-grown seedlings (E), flower (F), petal (G), and sepal (I). Scale bars represent 1 mm (A–C), 50 μm (D), 100 μm (E), and 400 μm (F–H).

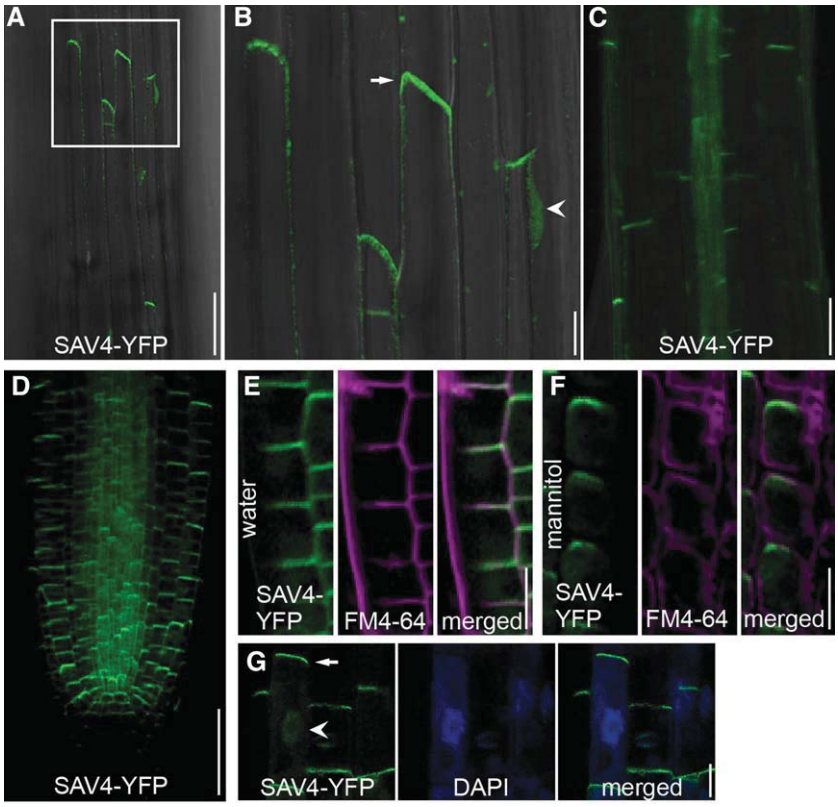

Figure 4. Subcellular localization of SAV4 in planta. A to D, Expression of SAV4-YFP in the hypocotyl epidermis (A and B) and vasculature (C), and in the root tip (D), indicating a dual localization of the protein at the plasma membrane and the nucleus. Shown in B is a magnification of the regions within the white box in A. E and F, Plasmolysis experiment showing that SAV4-YFP signals colocalize with the FM4-64-marked plasma membrane in roots of seedlings treated with water (E) and mannitol (F). G, SAV4-YFP signals overlap with DAPI in the root epidermal cells. White arrows indicate polarized shoot-side localization of SAV4, and white arrowheads mark nuclear SAV4. Scale bar = 50 μm (A, C, and D), 10 μm (B and E–G).

distinct localization patterns. We expressed C-terminal YFP-tagged SAV4 N-/C-terminal domain (n/cSAV4-YFP) under control of the cauliflower mosaic virus 35S promoter (Supplemental Fig. S4A). In the *35S::SAV4-YFP* transgenic seedlings, SAV4-YFP retained the polar plasma membrane localization, but no signal could be detected in the nucleus (Supplemental Fig. S4, B and E). Interestingly, nSAV4-YFP accumulated strongly in the nucleus (Supplemental Fig. S4, C and F), while cSAV4-YFP signal was detected in the cytoplasm and the plasma membrane, albeit without polarity (Supplemental Fig. S4, D and G). Results from the plasmolysis experiment confirmed that some of the cSAV4-YFP can still localize to the plasma membrane (Supplemental Fig. S4H). These data indicate that the N-terminal region of SAV4 may contain sequences conferring nuclear localization, while both the N- and C-terminal fragments determine SAV4 polar distribution at the plasma membrane. Whereas the wild-type SAV4-YFP complemented the *sav4* mutant, neither N- or C-terminal SAV4 rescued the short hypocotyl phenotype of *sav4* in shade (Supplemental Fig. S4I). We thus concluded that both regions of SAV4 were essential for its function. Since SAV4 expressed in the *35S::SAV4-YFP* line was only detected at the apical plasma membrane but not in the nucleus, we speculated that its localization at the plasma membrane makes major contribution to the function of SAV4 during the shade avoidance response.

To confirm the membrane localization of SAV4, we conducted subcellular fractionation experiments using 7-d-old light-grown *SAV4::SAV4-YFP* seedlings (Abas and Luschnig, 2010). As shown in Figure 5A, SAV4 was detected both in the microsomal fraction and soluble fraction, suggesting that SAV4 was associated with membranes. To further determine whether SAV4 was a peripheral membrane protein, pellets of microsomal fractions were treated with detergent Triton X-100, alkali buffer (pH 11), or high concentrations of salt (1 M NaCl). SAV4 could only be released from the membranes by solubilization with 1% Triton X-100 (Fig. 5B), indicating that the association between SAV4 and the membrane is rather strong.

The phenotype of the *sav4* mutant may be explained by altered PIN function, and PIN2 localizes to the apical membrane of epidermal cells, particularly since other PINs preferentially localize to other sides of the plasma membrane in root cells. We therefore determined whether the plasma membrane localization of SAV4 was PIN2 dependent in a *pin2* mutant background. However, we did not observe any differences in SAV4 distribution in the root epidermis cells when SAV4-YFP was expressed in *pin2* (Supplemental Fig. S5).

Altogether, these results indicate that SAV4, despite of lacking a discernible membrane anchoring motif, is truly targeted to the plasma membrane, and it is predominantly targeted to the side facing toward the shoot apical plasma membrane in a PIN2-independent manner.

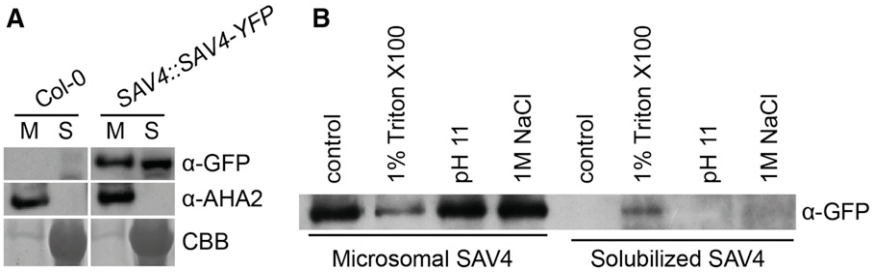

Figure 5. SAV4 protein is associated with the plasma membrane. A, Immunoblot analysis of SAV4 localization after cell fractionation of 7-d-old light-grown *SAV4::SAV4-YFP* seedlings. Microsomal (M) and soluble (S) fractions were separated by sodium dodecyl sulfate-polyacrylamide gel electrophoresis and subjected to western-blot analysis using α-GFP or α-Arabidopsis H^+-ATPASE2 (AHA2) antibodies. CBB, Coomassie Brilliant Blue-stained gel. B, The microsomal fraction obtained in A was solubilized by treating with 1% Triton X-100, carbonate buffer (pH 11), or 1 M NaCl. SAV4 proteins that were remained in the microsomal parts or solubilized by the treatment were subjected to the immunoblot analysis.

SAV4 Is Required for Basipetal Auxin Transport in Hypocotyls

Auxin is a key phytohormone required for shade-induced hypocotyl elongation (Steindler et al., 1999; Morelli and Ruberti, 2000). To examine if *sav4* was impaired in auxin biosynthesis, transport, or signaling, we tested the responses of *sav4* to picloram, an auxin analog, which is known to effectively stimulate hypocotyl elongation (Sorin et al., 2005). Two other previously identified *sav* mutants were included as controls: *sav3-1/taa1* contains a mutation in the auxin biosynthetic gene *TAA1* and *sav1-1/dwf4* contains a mutation in the brassinosteroid biosynthesis gene *DWARF4* (*DWF4*; Tao et al., 2008; Yu et al., 2015). As shown in Figure 6A, picloram rescued the short hypocotyl phenotype of *sav4* and *sav3-1/taa1*, but not that of the *sav1-1/dwf4*, suggesting that *sav4* may be defective in auxin biosynthesis or transport, but not in auxin signaling, and that auxin was indeed limiting for SAS in *sav4*. Since high temperatures can also promote hypocotyl elongation by increasing the level of endogenous free indole-3-acetic acid (IAA; Gray et al., 1998), the response of *sav4* to elevated temperatures was examined. As shown in Supplemental Figure S6A, *sav4* was defective in high-temperature-induced hypocotyl elongation, confirming that *sav4* is defective in the auxin pathway.

To directly examine whether the endogenous auxin level was altered in the *sav4* mutant, levels of free IAA were measured in 6-d-old seedlings grown in Wc and shade (Supplemental Fig. S6B). The results showed that free IAA levels of *sav4* in both light conditions were comparable to those of the wild type, indicating that *SAV4* may not be involved in IAA biosynthesis.

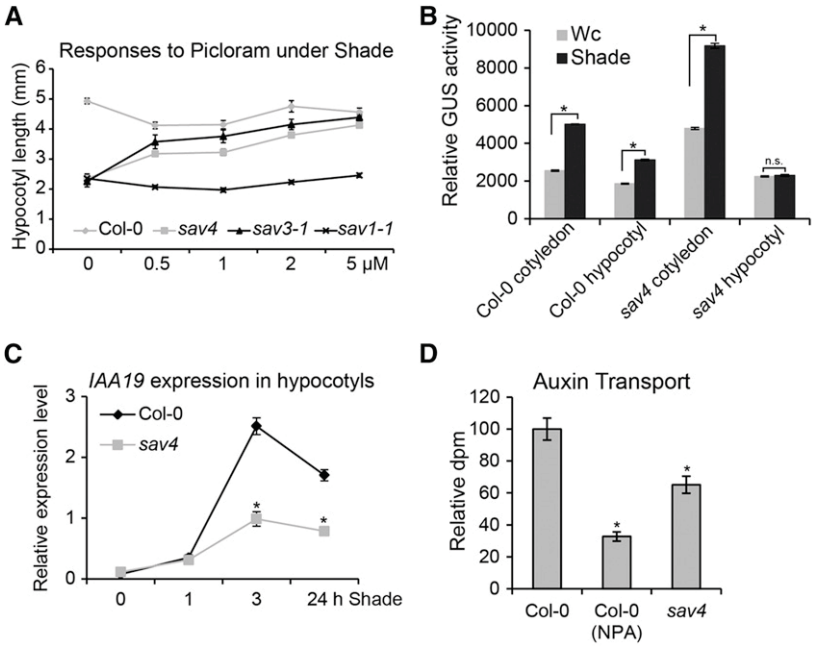

Figure 6. *sav4* Impairs polar auxin transport in the hypocotyl. A, Responses of *sav4* to picloram ($n \geq 20$). B, Quantitative analysis of GUS activity in the cotyledon/leaf primordia and hypocotyl of *sav4* and Col-0 transformed with the *DR5::GUS* reporter. Six-day-old seedlings were left in Wc or transferred to shade for 8 h ($n = 3$). C, Quantification of *IAA19* expression in the hypocotyl using qRT-PCR. Relative expression level as compared to a reference gene (At1g13320) is shown ($n = 3$). D, Basipetal auxin transport measurements of 4-d-old dark-grown seedlings. NPA (100 μM) strongly reduced the IAA transport of the wild type. Mean values from at least 12 replicate samples were determined, and the experiment was repeated three times with reproducible results. Error bars represent the SEM. Student's *t* test, compared with the wild type unless indicated with brackets: $^*P < 0.01$ and not significant (n.s.).

An auxin response-reporter line, *DR5::GUS*, is widely used to indirectly measure auxin distribution and responses (Sabatini et al., 1999; Aloni et al., 2003). To examine whether auxin distribution was altered in *sav4*, we crossed *DR5::GUS* into *sav4* and quantified *GUS* expression in cotyledons (including the two cotyledons and the first true leaf primordia) and hypocotyls. It was demonstrated that biosynthesis of auxin is enhanced in young leaves in response to shade and then transported to the hypocotyls, where it promotes hypocotyl elongation (Tao et al., 2008; Keuskamp et al., 2010). Indeed, GUS activity increased in both cotyledons and hypocotyls of the wild type after 8 h of shade treatment. However, such an increase was only detected in the cotyledons of *sav4*, not in the hypocotyls (Fig. 6B; Supplemental Fig. S6C). Furthermore, the expression of the *GUS* reporter in cotyledons was significantly higher in *sav4* than in the wild type under both Wc and shade, suggesting that transport of auxin from the young leaves to the hypocotyls may be reduced under both conditions. To further verify this hypothesis, we quantified the expression of the auxin- and shade-induced *IAA19* in hypocotyls using qRT-PCR (Keuskamp et al., 2010). As shown in Figure 6C, the expression of *IAA19* was strongly induced by shade in the wild type, while such induction was dramatically reduced in *sav4*. In the meantime, the expression of a shade marker gene, *PIF3-LIKE1* (*PIL1*), whose transcript level increases markedly in response to shade (Salter et al., 2003), was comparable between the wild type and *sav4* (Supplemental Fig. S6D). Together, these results indicate that phenotypes of *sav4* in shade may result from defects in the auxin pathway, which is likely due to an impaired auxin transport, but not auxin biosynthesis.

To verify the role of SAV4 in auxin transport, we directly measured basipetal auxin transport in hypocotyls of etiolated seedlings (Willige et al., 2013). In this assay, IAA transport in *sav4* was reduced by 40% compared to that in the wild type (Fig. 6D). Wild-type seedlings treated with the auxin transport inhibitor 1-*N*-naphthylphthalamic acid (NPA) also exhibited pronounced reduction in auxin transport, indicating that it was the active transport of IAA that was measured in our assay. We therefore conclude that SAV4 is indeed required for the basipetal auxin transport in hypocotyls.

To investigate whether *SAV4* transcript abundance could be regulated by auxin, we examined the expression of *SAV4* in response to auxins, including naphthylacetic acid, IAA, and 2,4-dichlorophenoxyacetic acid by qRT-PCR. As shown in Supplemental Figure S2C, the expression of *SAV4* was not significantly altered by these auxins, indicating that *SAV4* transcription may not be regulated by auxin.

The Influence of SAV4 on PIN3

PIN3 is a key player in low R:FR-induced hypocotyl elongation (Keuskamp et al., 2010). Transcription of *PIN3* is elevated in shade in an auxin-dependent manner, suggesting there is a positive feedback loop on auxin transport during shade (Keuskamp et al., 2010). We tested if SAV4 played a role in the regulation of PIN3 in shade. As shown in Figure 7A, shade-induced *PIN3* expression was significantly reduced in *sav4* compared to that in the wild type.

Subcellular localization of PIN3 is also changed from the basal end to the lateral side of the endodermal cells in the hypocotyl upon low R:FR treatment (Keuskamp et al., 2010). We crossed *sav4* with *PIN3::PIN3-GFP* and investigated if SAV4 was involved in shade-induced PIN3 repolarization (Zádniková et al., 2010). As previously reported, we observed that PIN3-GFP localized to the basal membranes of the endodermal cells in Wc and repolarized to the lateral side upon shade treatment

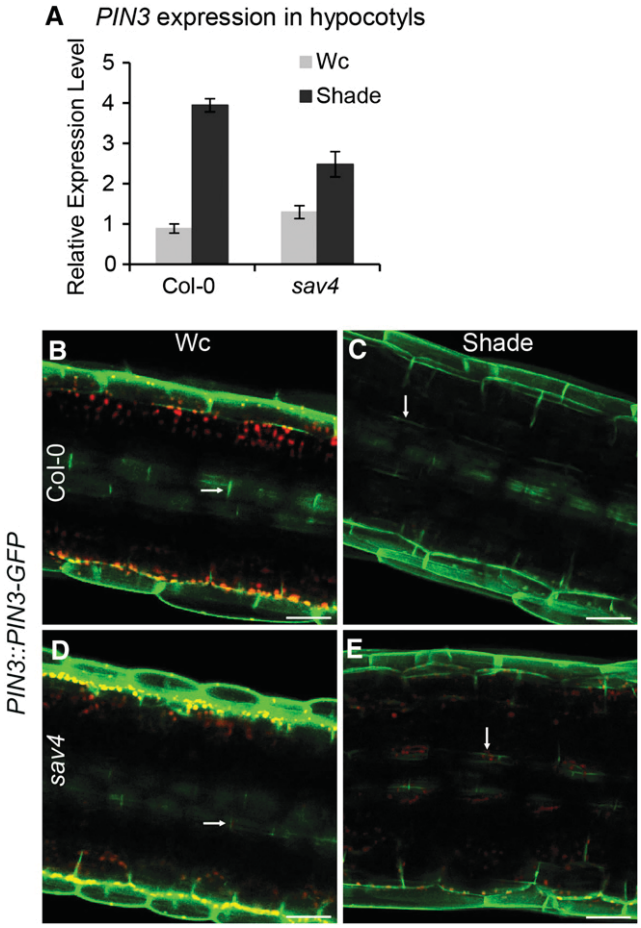

Figure 7. *PIN3* expression and PIN3-GFP localization in *sav4*. A, *PIN3* gene expression in hypocotyls upon 3 h of shade treatment. Relative expression level is shown (n = 3). Error bars represent the SEM. B to E, Using *PIN3::PIN3-GFP*, the subcellular localization of PIN3 was visualized in the wild type (B and C) and *sav4* (D and E). Six-day-old seedlings were transferred to shade (C and E) for 2 d and scanned by confocal microscope. The laser intensity was increased for obtaining a clear observation of seedlings grown in Wc (B and D). Arrows indicate localization of PIN3-GFP in the basal and lateral membranes of endodermal cells. Scale bar = 50 μm.

(Fig. 7, B and C). A similar pattern of PIN3-GFP repolarization occurred in *sav4*, although with an overall weaker fluorescence intensity in the vascular tissues (Fig. 7, D and E).

Phosphorylation of PIN proteins affects PIN localization or transporter activity (Friml et al., 2004; Willige et al., 2013; Zourelidou et al., 2014). To explore whether SAV4 influenced PIN3-mediated auxin transport directly, we examined the effects of SAV4 on PIN3 activation by D6PKs. SAV4 did not have any obvious effects on D6PK autophosphorylation or the transphosphorylation of PIN3 by D6PK (Supplemental Fig. S7A). Using a *Xenopus* oocyte system, we measured the influence of SAV4 on PIN3-mediated auxin transport and activation of PIN3 by D6PKs but found no significant effects (Supplemental Fig. S7B). We also examined PIN3 protein in etiolated seedlings, where phosphorylated PIN3 can be visualized as a shifted band and did not find any changes in PIN3 modification (Supplemental Fig. S7C). We thus concluded that SAV4 may not directly influence PIN3-mediated auxin efflux.

Taken together, these data suggest that defects of *sav4* in shade may result partially from reduced expression of *PIN3*, but not from altered localization or transporter activity of PIN3. As the shade-induced *PIN3* expression relies on the functional auxin pathway (Keuskamp et al., 2010), the above results further support a critical role of SAV4 in the auxin pathway.

SAV4 Modulates Auxin Efflux by Inhibiting ABCB Proteins

To investigate if the ABCB family of auxin transporters is required for the shade avoidance response, we examined phenotypes of *abcb1* and *abcb19* mutants in shade. As shown in Figure 8A, hypocotyls of both *abcb1* and *abcb19* mutants are shorter than the wild type in shade. *sav4 abcb1* or *sav4 abcb19* double mutants had further reduced hypocotyl lengths than either of the single mutants in shade. These observations indicate that ABCB-mediated auxin transport is required for shade-induced hypocotyl elongation and that there may be functional redundancy between ABCB1 and 19 during the shade avoidance responses.

To examine whether SAV4 influences IAA efflux activities of ABCBs, we employed a heterologous tobacco protoplast system. Consistent with published data (Henrichs et al., 2012), expression of ABCB1 and PIN1 effectively promoted IAA export from protoplasts

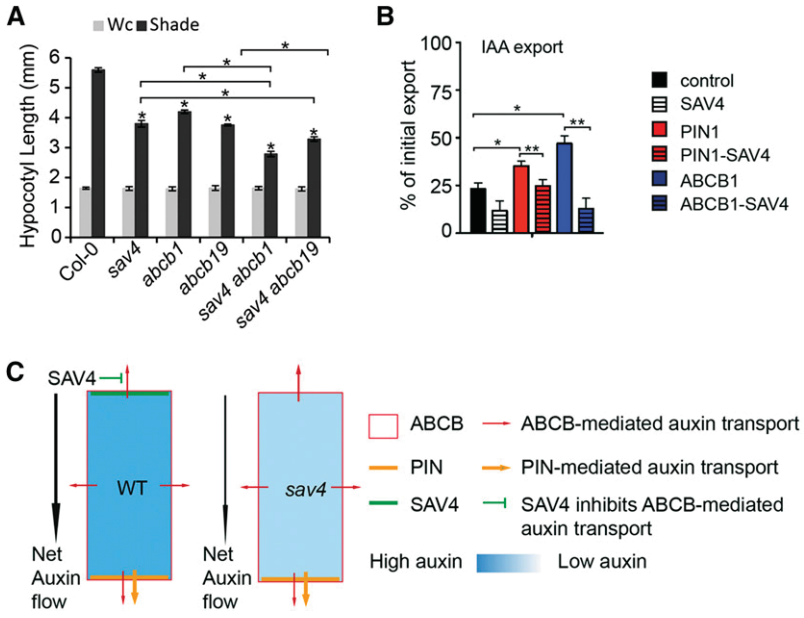

Figure 8. SAV4 inhibits ABCB1-mediated auxin efflux. A, Hypocotyl length of the wild type, *sav4*, *abcb1*, *abcb19*, *sav4 abcb1*, and *sav4 abcb19* mutants in Wc or simulated shade. Error bars represent the SEM ($n \geq 20$). Student's *t* test, compared with the wild-type Col-0 unless indicated with brackets: $^*P < 0.01$. B, Cotransfection of tobacco protoplasts with SAV4 negatively regulates PIN1- and ABCB1-mediated auxin (IAA) export. Significant differences (unpaired *t*-test with Welch's correction; *P*-value < 0.01) to vector control or to experiments without SAV4 are indicated by * and **, respectively ($n > 6$). C, Model for the molecular mechanism of SAV4 in the local auxin distribution. PINs reside at the rootward polar plasma membrane domains, which determines the directionality of auxin flow. ABCBs that target to the plasma membrane in a nonpolar manner interact with PINs at the polar domain and contribute to generate an effective auxin stream from the shoot to the hypocotyl. Shootward-localized SAV4 is able to block ABCB-mediated auxin efflux, thus controlling the cellular auxin pool available for PIN-mediated polar auxin transport. In *sav4*, apical ABCB-mediated auxin efflux might be increased, which leads to a reduction in cellular auxin levels and decreased net basipetal auxin flow.

(Fig. 8B). Expression of SAV4 alone slightly inhibited IAA export, which suggests that it may inhibit endogenous transporter activities. Protoplasts transformed with both SAV4 and PIN1 exhibited reduced IAA export compared to those transformed with PIN1 alone, but export was still higher than those transformed with SAV4 alone. Furthermore, the reduction level was comparable to that observed when protoplasts were transformed with or without SAV4. Thus, SAV4 may have limited effects on PIN1-mediated auxin efflux. On the other hand, protoplasts transformed with SAV4 and ABCB1 exhibited significantly reduced IAA efflux compared to those transformed with ABCB1, which is comparable to those transformed with SAV4 alone. This result indicates that SAV4 inhibits ABCB1-mediated auxin efflux in the protoplast system. As SAV4 localizes to the apical side of the cell, we further hypothesize that mutation in SAV4 may affect acropetal auxin transport in hypocotyls. To test this idea, we measured acropetal auxin transport in hypocotyls. Compared to the wild type, acropetal transport of IAA and naphthylacetic acid increased significantly in the *sav4* mutant, while mutation in *ABCB* or *PIN3* had negligible effects on acropetal auxin transport (Supplemental Fig. S7D). Increased acropetal auxin transport in *sav4* hypocotyls is consistent with our hypothesis and verifies an inhibitory impact of SAV4 on ABCB transport activity found on the cellular level also in the tissue context.

DISCUSSION

SAV4 Is Required for Polar Auxin Transport

In this study, we identify SAV4 as a novel protein required for shade avoidance responses in Arabidopsis. We further present several lines of evidence to demonstrate a role for SAV4 in auxin transport and auxin transport-dependent growth during shade-induced hypocotyl elongation. *sav4* was identified in a forward genetic screen as a mutant defective in shade-induced hypocotyl elongation. As *sav4* was also impaired in the high temperature-induced hypocotyl elongation, a process that is specifically regulated by auxin (Gray et al., 1998), we then focused on the role of SAV4 in the auxin pathway. Increased auxin biosynthesis, intact auxin signaling, and auxin transport are all required for shade-induced hypocotyl elongation (Tao et al., 2008; Keuskamp et al., 2010). Our results showed that exogenous application of an auxin analog, picloram, could rescue the hypocotyl elongation defect of *sav4* under shade, which led us to speculate that *sav4* may be defective in auxin biosynthesis or transport, but not in auxin signaling (Fig. 6A). Shade-induced rapid IAA biosynthesis was normal in *sav4* mutant seedlings (Supplemental Fig. S6B), suggesting that SAV4 may not be involved in IAA biosynthesis. To determine whether *sav4* was defective in auxin transport, we examined the expression of both the auxin reporter gene *DR5::GUS* and the auxin-responsive gene *IAA19* in hypocotyls. Shade-induced expression of these genes was specifically reduced in hypocotyls of *sav4* compared with those in the wild type (Fig. 6, B and C; Supplemental Fig. S6C). Finally, results from direct measurement of basipetal auxin transport using dark-grown seedlings demonstrated that *sav4* is defective in basipetal hypocotyl auxin transport in hypocotyls (Fig. 6D). Together, these results indicate that SAV4 is required for proper auxin transport in hypocotyls.

SAV4 Is a Novel Regulator of Auxin Transport

sav4 contains a mutation in *At5G10200* encoding a novel protein with no homology to any other protein of known function in Arabidopsis. Proteins sharing high homology with SAV4 can be found in *Oryza sativa* and *Zea mays*, implicating that SAV4 homologs are present in both dicots and monocots (Fig. 2D). Results from the tissue-specific expression pattern analyses in light-grown seedlings showed that SAV4 was not only highly expressed in hypocotyls, but also showed strong expression in emerging new leaves, root tips, carpels, sepals, filaments of the stamen, and the vascular tissues (Fig. 3), suggesting that SAV4 may regulate auxin distribution in those tissues as well.

The SAV4-YFP fusion protein expressed from the *SAV4* promoter localized to both the plasma membrane and the nucleus (Fig. 4). Membrane-localized SAV4-YFP fluorescence displayed polar distribution at the apical plasma membrane. Cell fractionation experiments confirmed the membrane localization of SAV4 (Fig. 5). Since no putative transmembrane domain can be predicted from the sequence analyses of SAV4 (http://ch.embnet.org/software/TMPRED_form.html), we performed a series of truncation analyses. The truncated SAV4 containing the N-terminal or C-terminal region was detected in the nucleus or the cytoplasm and the plasma membrane, respectively, indicating that both regions of SAV4 are essential for its polar plasma membrane localization (Supplemental Fig. S4, B−G). Interestingly, SAV4-YFP expressed under the 35S promoter was only visible on the plasma membrane yet was able to rescue the short hypocotyl phenotype of *sav4* in shade. Neither the nSAV4-YFP nor the cSAV4-YFP rescued *sav4* (Supplemental Fig. S4I), suggesting that polar plasma membrane-localized SAV4 may be critical for its function. Moreover, the fact that the polar targeting of SAV4 was retained in the *pin2* epidermal root cells indicated that SAV4 does not achieve its polar localization through colocalizing with PIN.

Palmitoylation, known as S-acylation, involves the reversible addition of fatty acids to proteins, which increases their membrane association. Recently, palmitoylation has been demonstrated to be implicated in a multitude of cellular functions in plants, including vesicle trafficking, cell polarization, hormone signaling, and disease resistance (Hemsley, 2015). For instance, ROP6 is a small G-protein involved in signal transduction and polarized growth. The activated

(GTP-bound) and S-acylated ROP6 partitions into detergent-resistant membranes, whereas the inactive (GDP-bound), non-S-acylated form associates with the detergent-soluble membranes. This acylation-dependent membrane localization is indispensable for ROP6 function (Sorek et al., 2007). Using the CSS-Palm program (http://csspalm.biocuckoo.org/index.php; Ren et al., 2008), we found that SAV4 protein contains two Cys residues in the N-terminal region, which are predicted to be palmitoylated with a high score. Future research will have to uncover how SAV4 is targeted to different cellular compartments and whether the hypothetical acylation affects SAV4 localization and function.

Model of SAV4 in Establishing Proper Auxin Gradients

PIN3 plays a critical role in the auxin transport and hypocotyl elongation in low R:FR (Keuskamp et al., 2010). To unravel how SAV4 participates in polar auxin transport, the abundance and localization of PIN3 was investigated. Although *sav4* displayed a pronounced reduction in the transcript levels of PIN3, the repolarization of PIN3 seemed unaffected upon shade treatment. However, we cannot rule out the possibility that *SAV4* mutation may alter the dynamics of PIN3 turnover or polarization in shade. Furthermore, SAV4 does not seem to directly affect the auxin transport activity of PIN3 (Supplemental Fig. S7B). We thus speculate that SAV4 may not affect auxin transport by directly modulating PIN3-mediated auxin efflux. The decreased level of PIN3 transcript in *sav4* may result from reduced auxin levels in hypocotyls of *sav4*.

ABCBs represent another subgroup of auxin transporters, and they are supposed to export auxin in a nonpolar manner because of their nonpolar cellular localization (Geisler et al., 2005; Mravec et al., 2008). Considering that SAV4 and ABCB1 colocalize at the apical plasma membrane, we examined whether SAV4 influenced ABCB1-mediated auxin efflux. Coexpression of SAV4 and ABCB1 in tobacco protoplasts showed that ABCB1-mediated auxin efflux was dramatically reduced by SAV4. Furthermore, both *sav4* and *abcb* mutants exhibited reduced basipetal auxin transport (Fig. 6D; Noh et al., 2001) and hypocotyl elongation defects under shade (Fig. 8A). Therefore, we propose that in hypocotyls (Fig. 8C), SAV4 inhibits ABCB-mediated auxin efflux at the apical membrane and, thus, controls the available cellular auxin for basipetal auxin transport. In the *sav4* mutant, apical ABCB-mediated auxin efflux might be enhanced, which leads to a reduction in cellular auxin levels compared to the wild type and decreased net basipetal auxin flow as measured in the hypocotyl basipetal auxin transport experiment. According to this model, SAV4 would promote basipetal auxin transport by inhibiting acropetal ABCB1-mediated transport, and acropetal auxin transport in hypocotyls may increase in the *sav4* mutant, which was indeed observed in the acropetal auxin transport assay (Supplemental Fig. S7D).

It was recently shown that during hypocotyl phototropism, the photoreceptor kinase PHOT1 phosphorylates ABCB19 and inhibits its efflux activity, which consequently leads to a transient increase in auxin levels in the hypocotyl apex and allows auxin redistribution to the epidermis through PIN3-mediated auxin efflux (Christie et al., 2011). The authors proposed that ABCB19 is required for long-distance auxin transport streams. It was suggested that during the shade avoidance response, auxin synthesized in cotyledons and young leaves was first transported to the hypocotyls and then redistributed to the epidermis through PIN3-mediated auxin efflux (Tao et al., 2008; Keuskamp et al., 2010). Through analyzing the expression of *DR5::GUS*, we observed that shade treatment significantly increased GUS expression in both vasculature and outer tissues of the hypocotyls, presumably the epidermis, while such enhanced expression was not seen in the *sav4* mutant (Supplemental Fig. S6C). Thus, although PHOT1 and SAV4 inhibit ABCB-mediated auxin efflux through different molecular mechanisms, they seem both to act in concert with PINs by modulating long-distance auxin transport streams.

SAV4 is predicted to harbor an ARM repeat- and a TPR-like domain, both of which are involved in protein-protein interactions and assembly of multiprotein complexes. The FKBP42, TWISTED DWARF1, interacts with ABCB and ABCC transporters at the plasma membrane or the vacuolar membrane via its PPIase-like domain and TPR repeats, respectively (Geisler et al., 2003, 2004). This interaction was essential for maintaining ABCB-mediated long-distance auxin transport (Wang et al., 2013). Although the underlying mechanisms of such regulations are unknown, these protein-protein interactions may represent an additional level of regulation on auxin transport. Future studies will have to reveal how SAV4 interacts with ABCBs and whether SAV4 inhibits ABCB-mediated auxin efflux directly.

MATERIALS AND METHODS

Plant Materials and Growth Conditions

The transgenic lines and mutants used for crossing with *sav4* were as follows: *DR5::GUS* (Sabatini et al., 1999); *PIN3::PIN3-GFP* (Zádniková et al., 2010); *sav3-1* and *sav1-1* (Tao et al., 2008); *abcb1* (SALK_046440); and *abcb19* (SALK_033455). To clear the genetic background, *sav4* was backcrossed six times with the wild-type Col-0; only progenies of *sav4* (B6F2) were used in the phenotypic analyses. For complementation experiments, the genomic *SAV4* sequences, including 1.5 kb of upstream sequences and 900 bp of downstream sequences, were PCR amplified from the wild-type genomic DNA and cloned into the *pJHA212K* vector using *Bam*HI and *Eco*RI sites. For the expression and localization analyses of *SAV4*, the 900 bp downstream sequences of genomic *SAV4* DNA were cloned into the *pJHA212K-GUS/YFP* vectors using *Sal*I/*Hin*dIII; then the genomic *SAV4* DNA, including 1.5 kb of upstream sequences, was inserted using the *Bam*HI/*Eco*RI sites. For the truncation analyses, full-length and truncated *SAV4* cDNA were amplified from the wild-type cDNA library and then cloned into the *pCHF3-YFP* vector (CaMV 35S promoter). Primer sequences are provided in Supplemental Table S1.

Seeds were usually surface-sterilized in ethanol and grown on half-strength Murashige and Skoog media with 0.8% agar, then stratified at 4°C for 3 d unless stated otherwise. All seedlings were grown in Wc at 22°C. For the shade

treatment/high temperature, seedlings were grown in Wc light at 22°C for 6 d, then transferred to the simulated shade (red: 13 μmol m^{-2} s^{-1}, blue: 3.5 μmol m^{-2} s^{-1}, far red: 21 μmol m^{-2} s^{-1}) or 29°C for additional 3 d. For the responses to picloram (Sigma), seedlings were grown on half-strength Murashige and Skoog supplemented with different concentrations of picloram for 6 d under Wc. The plates were transferred to the simulated shade for 3 d before measuring the hypocotyl length using Scion Image software (http://www.scioncorp.com). For the monochromatic light responses, sterilized seeds were stratified in 4°C for 3 d, then exposed to Wc for 2 h and transferred to dark or the respective light conditions for 3 d before the hypocotyl length measurement.

RNA Isolation and qRT-PCR Analysis

Total RNAs were extracted following Roche TriPure RNA isolation protocol (www.roche-applied-science.com). One microgram of total RNAs were reverse transcribed using the First Strand cDNA Synthesis Kit (Thermo). qRT-PCR was performed using the SYBR green method with a Stratagene Mx3000P real-time system cycler (Agilent). A 40-cycle, three-step amplification protocol (10 s at 95°C, 20s at 60°C, and 25 s at 72°C) was used for all measurement. *REF3* (At1g13320) was used as a reference gene (Czechowski et al., 2005). Fold change was then calculated by setting the relative expression of the gene in Col-0 or untreated control samples to one (Zhang et al., 2016). SE was calculated from three replicates. Primer sequences are provided in Supplemental Table S1.

Histochemical Assays and GUS Activity Measurement

GUS activity was detected by histological GUS staining method. Seedlings were fixed in 90% acetone for 15 min, washed twice with 100 mM Na-phosphate buffer, pH 7.2, and incubated overnight in staining solution [100 mM Na-phosphate buffer, pH 7.2, 2 mM $K_4Fe(CN)_6$, 2 mM $K_3Fe(CN)_6$, 0.1% (v/v) Triton X-100, 2 mM X-Gluc (5-bromo-4-chloro-3-indolyl β-D-glucoronide)]. Thereafter, seedlings were cleared in 70% ethanol and examined using the microscope (Leica DM2500).

For quantification of GUS activity, total proteins were prepared using the GUS extraction buffer (50 mM Na-phosphate buffer, pH 7.2,10 mM DTT, 10 mM EDTA, 0.1% sarcosyl, 0.1% Triton X-100). At least 15 μg of total proteins were used for GUS assay in solution containing the MUG (4-methylumbelliferyl-beta-D-glucuronide, Sigma). After incubation at 37°C for 45 min, the reaction was stopped by adding 0.2 M Na_2CO_3 and the amount of product was measured using a fluorometer (Cary Eclipse). Relative GUS activity was calculated by normalizing to the amount of total protein determined by the Bradford assay. Three biological replicates were included in each experiment.

Cell Biology

For subcellular localization analyses, 5-day-old light-grown and 2-day-old etiolated seedlings were used to visualize the localization of SAV4-YFP in the root tip and hypocotyl with confocal laser scanning microscopy (Zeiss LSM 780). FM4-64 (3 μM) was included to label the plasma membrane. DAPI (1–2 μg/mL) was used to label the nuclei. For the plasmolysis experiment, *SAV4::SAV4-YFP* plants were treated with either water (control) or 0.8 M mannitol for 10 min before analysis. To image the expression pattern of *PIN3::PIN3-GFP* in the hypocotyl, 6-d-old Wc-grown seedlings were transferred to shade for 2 d. Subsequently, confocal images were acquired from the middle-up hypocotyl region according to the methods described (Keuskamp et al., 2010). Various confocal settings were set to record the emission of GFP (excitation at 488 nm; emission of 493–540 nm), YFP (excitation at 514 nm; emission of 520–560 nm), FM4-64 (excitation at 561 nm; emission of 580–660 nm), DAPI (excitation at 405 nm; emission of 410–470 nm), and the chlorophyll fluorescence (excitation at 561 nm; emission of 570–650 nm).

Protein Extraction and Immunoblotting

For the subcellular fractionation, materials from 7-d-old light-grown transgenic plants (*SAV4::SAV4-YFP*) were used to extract the soluble and microsomal fractions according to a method described by Abas and Luschnig (2010). In brief, approximately 100 mg of fresh plant material was collected and frozen in liquid nitrogen. The frozen samples were homogenized in extraction buffer (100 mM Tris-HCl, pH 7.5, 0.81 M Suc, 5% glycerol, 10 mM EDTA, 10 mM EGTA, 5 mM KCl, 40 μM MG132, 1 mM PMSF, and complete EDTA-free protease inhibitor) and subjected to centrifugation (600 $\times$ *g*, 3 min) at least two times. The cleared supernatants were diluted with water (make final Suc concentrations from 24%–27% to 12%–13%) and centrifuged at 21,000 $\times$ *g* for 1.5 to 2 h in a refrigerated MCF (Eppendorf Centrifuge 5417R). The supernatant was carefully removed for analysis of the soluble fraction, and the microsomal pellets were washed with the wash buffer (20 mM Tris-HCl, pH 7.5, 5 mM EDTA, 5 mM EGTA, 1 mM PMSF, and complete EDTA-free protease inhibitor). Otherwise, the wash buffer was supplied with 1% Triton X-100, carbonate buffer (pH 11) or 1 M NaCl. The microsomal pellets were recentrifuged at 21,000 $\times$ *g* for 45 min and finally were solubilized into 2$\times$ Laemmli buffer (125 mM Tris-HCl, pH 6.8, 20% glycerol, 4% SDS, 0.0005% bromophenol blue, and 1.4% β-mercaptoethanol). The proteins were subsequently separated on 10% SDS-PAGE and used for immunoblotting. Primary anti-GFP (1: 2000, Transgene), anti-AHA2 (1:1000, Agrisera), and secondary anti-mouse (1: 2000, Beyotime) antibodies were used.

Auxin Transport Measurement

For basipetal hypocotyl auxin transport measurements, we followed a previously published protocol (Willige et al., 2013). In brief, 4-d-old etiolated seedlings grown vertically on square plates were transferred to new plates containing Parafilm strips and positioned such that 5 mm of the apical parts of the seedlings were on the Parafilm. Then a 0.5 μL droplet of [^{3}H]IAA solution (417 nM [^{3}H]IAA, 5 mM MES, 1% glycerol) was applied to the cotyledons of each seedling. NPA (100 μM) was included as the negative control. The plates were placed vertically in the dark for 6 h. After that, the part of each seedling below the apical 5-mm segments was dissected, and three seedlings were pooled together and measured in 3 mL QuicksafeA scintillation liquid in a liquid scintillation analyzer (Tri Carb 2100TR; Perkin-Elmer). [^{3}H]IAA (20 Ci/mmol) was purchased from American Radiolabeled Chemicals (ART 0340). The experiment was repeated three times with reproducible results, and one representative result was shown.

IAA export from tobacco (*Nicotiana benthamiana*) protoplasts after *Agrobacterium*-mediated leaf transfection was analyzed as described previously (Henrichs et al., 2012). Relative export from protoplasts was calculated from exported radioactivity as follows: (radioactivity in the protoplasts at time t = x min) − (radioactivity in the protoplasts at time t = 0) $\times$ (100%)/(radioactivity in the protoplasts at t = 0 min).

Phylogenetic Analysis

A neighbor joining phylogenetic tree depicting the relationship of SAV4 with orthologs in other plant species was drawn based on the alignment with MEGA.

Accession Numbers

Sequence data from this article can be found in the GenBank/EMBL data libraries under the following accession numbers: SAV4 (At5g10200), REF3 (At1g13320), IAA19 (At3g15540), PIN3 (At1g70940), PIN1 (At1g73590), *PIL1* (At2g46970), SAV3 (At1g70560), SAV1 (At3g19820), D6PK (At5g55910), ABCB1 (At2g36910), and ABCB19 (At3g28860).

Supplemental Data

The following supplemental materials are available.

Supplemental Figure S1. Phenotypes of *sav4*.

Supplemental Figure S2. Expression analysis of *SAV4*.

Supplemental Figure S3. Z-stacks of hypocotyls of *SAV4::SAV4-YFP* from epidermis into vasculature.

Supplemental Figure S4. Specific domains of SAV4 determine its localization and function.

Supplemental Figure S5. Polar targeting of SAV4 is unaltered in *pin2* mutant.

Supplemental Figure S6. *sav4* is normal in auxin biosynthesis.

Supplemental Figure S7. SAV4 is not directly involved in D6PK-activated PIN3-mediated auxin efflux

Supplemental Table S1. Primers used in this study.

ACKNOWLEDGMENTS

We thank Inês C.R. Barbosa (Technische Universität München), Benjamin Weller (Technische Universität München), Laurence Charrier (University of Fribourg), and Roger Granbom (Swedish University of Agricultural Sciences) for skillful technical assistance, and Wei Xu (Third Institute of Oceanography, State Oceanic Administration) for helping with the phylogenetic analyses.

Received September 27, 2016; accepted November 17, 2016; published November 21, 2016.

LITERATURE CITED

Abas L, Luschnig C (2010) Maximum yields of microsomal-type membranes from small amounts of plant material without requiring ultracentrifugation. Anal Biochem **401:** 217–227

Aloni R, Schwalm K, Langhans M, Ullrich CI (2003) Gradual shifts in sites of free-auxin production during leaf-primordium development and their role in vascular differentiation and leaf morphogenesis in Arabidopsis. Planta **216:** 841–853

Barbosa IC, Zourelidou M, Willige BC, Weller B, Schwechheimer C (2014) D6 PROTEIN KINASE activates auxin transport-dependent growth and PIN-FORMED phosphorylation at the plasma membrane. Dev Cell **29:** 674–685

Benjamins R, Quint A, Weijers D, Hooykaas P, Offringa R (2001) The PINOID protein kinase regulates organ development in Arabidopsis by enhancing polar auxin transport. Development **128:** 4057–4067

Benschop JJ, Mohammed S, O'Flaherty M, Heck AJ, Slijper M, Menke FL (2007) Quantitative phosphoproteomics of early elicitor signaling in Arabidopsis. Mol Cell Proteomics **6:** 1198–1214

Blakeslee JJ, Bandyopadhyay A, Lee OR, Mravec J, Titapiwatanakun B, Sauer M, Makam SN, Cheng Y, Bouchard R, Adamec J, et al (2007) Interactions among PIN-FORMED and P-glycoprotein auxin transporters in Arabidopsis. Plant Cell **19:** 131–147

Casal JJ (2013) Photoreceptor signaling networks in plant responses to shade. Annu Rev Plant Biol **64:** 403–427

Christie JM, Yang H, Richter GL, Sullivan S, Thomson CE, Lin J, Titapiwatanakun B, Ennis M, Kaiserli E, Lee OR, et al (2011) phot1 inhibition of ABCB19 primes lateral auxin fluxes in the shoot apex required for phototropism. PLoS Biol **9:** e1001076

Cole B, Kay SA, Chory J (2011) Automated analysis of hypocotyl growth dynamics during shade avoidance in Arabidopsis. Plant J **65:** 991–1000

Czechowski T, Stitt M, Altmann T, Udvardi MK, Scheible WR (2005) Genome-wide identification and testing of superior reference genes for transcript normalization in Arabidopsis. Plant Physiol **139:** 5–17

Dhonukshe P, Huang F, Galvan-Ampudia CS, Mähönen AP, Kleine-Vehn J, Xu J, Quint A, Prasad K, Friml J, Scheres B, et al (2010) Plasma membrane-bound AGC3 kinases phosphorylate PIN auxin carriers at TPRXS(N/S) motifs to direct apical PIN recycling. Development **137:** 3245–3255

Franklin KA, Whitelam GC (2005) Phytochromes and shade-avoidance responses in plants. Ann Bot (Lond) **96:** 169–175

Friml J, Wiśniewska J, Benková E, Mendgen K, Palme K (2002) Lateral relocation of auxin efflux regulator PIN3 mediates tropism in Arabidopsis. Nature **415:** 806–809

Friml J, Yang X, Michniewicz M, Weijers D, Quint A, Tietz O, Benjamins R, Ouwerkerk PB, Ljung K, Sandberg G, et al (2004) A PINOID-dependent binary switch in apical-basal PIN polar targeting directs auxin efflux. Science **306:** 862–865

Geisler M, Blakeslee JJ, Bouchard R, Lee OR, Vincenzetti V, Bandyopadhyay A, Titapiwatanakun B, Peer WA, Bailly A, Richards EL, et al (2005) Cellular efflux of auxin catalyzed by the Arabidopsis MDR/PGP transporter AtPGP1. Plant J **44:** 179–194

Geisler M, Girin M, Brandt S, Vincenzetti V, Plaza S, Paris N, Kobae Y, Maeshima M, Billion K, Kolukisaoglu UH, et al (2004) Arabidopsis immunophilin-like TWD1 functionally interacts with vacuolar ABC transporters. Mol Biol Cell **15:** 3393–3405

Geisler M, Kolukisaoglu HU, Bouchard R, Billion K, Berger J, Saal B, Frangne N, Koncz-Kalman Z, Koncz C, Dudler R, et al (2003) TWISTED DWARF1, a unique plasma membrane-anchored immunophilin-like protein, interacts with Arabidopsis multidrug resistance-like transporters AtPGP1 and AtPGP19. Mol Biol Cell **14:** 4238–4249

Gray WM, Ostin A, Sandberg G, Romano CP, Estelle M (1998) High temperature promotes auxin-mediated hypocotyl elongation in Arabidopsis. Proc Natl Acad Sci USA **95:** 7197–7202

Hemsley PA (2015) The importance of lipid modified proteins in plants. New Phytol **205:** 476–489

Henrichs S, Wang B, Fukao Y, Zhu J, Charrier L, Bailly A, Oehring SC, Linnert M, Weiwad M, Endler A, et al (2012) Regulation of ABCB1/PGP1-catalysed auxin transport by linker phosphorylation. EMBO J **31:** 2965–2980

Hersch M, Lorrain S, de Wit M, Trevisan M, Ljung K, Bergmann S, Fankhauser C (2014) Light intensity modulates the regulatory network of the shade avoidance response in Arabidopsis. Proc Natl Acad Sci USA **111:** 6515–6520

Huang F, Zago MK, Abas L, van Marion A, Galván-Ampudia CS, Offringa R (2010) Phosphorylation of conserved PIN motifs directs Arabidopsis PIN1 polarity and auxin transport. Plant Cell **22:** 1129–1142

Keuskamp DH, Pollmann S, Voesenek LA, Peeters AJ, Pierik R (2010) Auxin transport through PIN-FORMED 3 (PIN3) controls shade avoidance and fitness during competition. Proc Natl Acad Sci USA **107:** 22740–22744

Mashiguchi K, Tanaka K, Sakai T, Sugawara S, Kawaide H, Natsume M, Hanada A, Yaeno T, Shirasu K, Yao H, et al (2011) The main auxin biosynthesis pathway in Arabidopsis. Proc Natl Acad Sci USA **108:** 18512–18517

Morelli G, Ruberti I (2000) Shade avoidance responses. Driving auxin along lateral routes. Plant Physiol **122:** 621–626

Mravec J, Kubes M, Bielach A, Gaykova V, Petrásek J, Skůpa P, Chand S, Benková E, Zazímalová E, Friml J (2008) Interaction of PIN and PGP transport mechanisms in auxin distribution-dependent development. Development **135:** 3345–3354

Müller A, Guan C, Gälweiler L, Tänzler P, Huijser P, Marchant A, Parry G, Bennett M, Wisman E, Palme K (1998) AtPIN2 defines a locus of Arabidopsis for root gravitropism control. EMBO J **17:** 6903–6911

Noh B, Murphy AS, Spalding EP (2001) Multidrug resistance-like genes of Arabidopsis required for auxin transport and auxin-mediated development. Plant Cell **13:** 2441–2454

Pencík A, Simonovik B, Petersson SV, Henyková E, Simon S, Greenham K, Zhang Y, Kowalczyk M, Estelle M, Zazímalová E, et al (2013) Regulation of auxin homeostasis and gradients in Arabidopsis roots through the formation of the indole-3-acetic acid catabolite 2-oxindole-3-acetic acid. Plant Cell **25:** 3858–3870

Péret B, Swarup K, Ferguson A, Seth M, Yang Y, Dhondt S, James N, Casimiro I, Perry P, Syed A, et al (2012) AUX/LAX genes encode a family of auxin influx transporters that perform distinct functions during Arabidopsis development. Plant Cell **24:** 2874–2885

Petrasek J, Friml J (2009) Auxin transport routes in plant development. Development **136:** 2675–2688

Petrásek J, Mravec J, Bouchard R, Blakeslee JJ, Abas M, Seifertová D, Wisniewska J, Tadele Z, Kubes M, Covanová M, et al (2006) PIN proteins perform a rate-limiting function in cellular auxin efflux. Science **312:** 914–918

Procko C, Burko Y, Jaillais Y, Ljung K, Long JA, Chory J (2016) The epidermis coordinates auxin-induced stem growth in response to shade. Genes Dev **30:** 1529–1541

Ren J, Wen L, Gao X, Jin C, Xue Y, Yao X (2008) CSS-Palm 2.0: an updated software for palmitoylation sites prediction. Protein Eng Des Sel **21:** 639–644

Sabatini S, Beis D, Wolkenfelt H, Murfett J, Guilfoyle T, Malamy J, Benfey P, Leyser O, Bechtold N, Weisbeek P, et al (1999) An auxin-dependent distal organizer of pattern and polarity in the Arabidopsis root. Cell **99:** 463–472

Salter MG, Franklin KA, Whitelam GC (2003) Gating of the rapid shade-avoidance response by the circadian clock in plants. Nature **426:** 680–683

Savaldi-Goldstein S, Peto C, Chory J (2007) The epidermis both drives and restricts plant shoot growth. Nature **446:** 199–202

Sorek N, Poraty L, Sternberg H, Bar E, Lewinsohn E, Yalovsky S (2007) Activation status-coupled transient S acylation determines membrane partitioning of a plant Rho-related GTPase. Mol Cell Biol **27:** 2144–2154

Sorin C, Bussell JD, Camus I, Ljung K, Kowalczyk M, Geiss G, McKhann H, Garcion C, Vaucheret H, Sandberg G, et al (2005) Auxin and light control of adventitious rooting in Arabidopsis require ARGONAUTE1. Plant Cell **17:** 1343–1359

Steindler C, Matteucci A, Sessa G, Weimar T, Ohgishi M, Aoyama T, Morelli G, Ruberti I (1999) Shade avoidance responses are mediated by the ATHB-2 HD-zip protein, a negative regulator of gene expression. Development **126:** 4235–4245

Swarup R, Péret B (2012) AUX/LAX family of auxin influx carriers-an overview. Front Plant Sci **3:** 225

Tao Y, Ferrer JL, Ljung K, Pojer F, Hong F, Long JA, Li L, Moreno JE, Bowman ME, Ivans LJ, et al (2008) Rapid synthesis of auxin via a new tryptophan-dependent pathway is required for shade avoidance in plants. Cell **133:** 164–176

Titapiwatanakun B, Blakeslee JJ, Bandyopadhyay A, Yang H, Mravec J, Sauer M, Cheng Y, Adamec J, Nagashima A, Geisler M, et al (2009) ABCB19/PGP19 stabilises PIN1 in membrane microdomains in Arabidopsis. Plant J **57:** 27–44

Vanneste S, Friml J (2009) Auxin: a trigger for change in plant development. Cell **136:** 1005–1016

Vieten A, Sauer M, Brewer PB, Friml J (2007) Molecular and cellular aspects of auxin-transport-mediated development. Trends Plant Sci **12:** 160–168

Wang B, Bailly A, Zwiewka M, Henrichs S, Azzarello E, Mancuso S, Maeshima M, Friml J, Schulz A, Geisler M (2013) Arabidopsis TWISTED DWARF1 functionally interacts with auxin exporter ABCB1 on the root plasma membrane. Plant Cell **25:** 202–214

Willige BC, Ahlers S, Zourelidou M, Barbosa IC, Demarsy E, Trevisan M, Davis PA, Roelfsema MR, Hangarter R, Fankhauser C, et al (2013) D6PK AGCVIII kinases are required for auxin transport and phototropic hypocotyl bending in Arabidopsis. Plant Cell **25:** 1674–1688

Wisniewska J, Xu J, Seifertová D, Brewer PB, Ruzicka K, Blilou I, Rouquié D, Benková E, Scheres B, Friml J (2006) Polar PIN localization directs auxin flow in plants. Science **312:** 883

Yu J, Qiu H, Liu X, Wang M, Gao Y, Chory J, Tao Y (2015) Characterization of tub4(P287L), a β-tubulin mutant, revealed new aspects of microtubule regulation in shade. J Integr Plant Biol **57:** 757–769

Zádníková P, Petrásek J, Marhavy P, Raz V, Vandenbussche F, Ding Z, Schwarzerová K, Morita MT, Tasaka M, Hejátko J, et al (2010) Role of PIN-mediated auxin efflux in apical hook development of Arabidopsis thaliana. Development **137:** 607–617

Zhang Y, Wen C, Liu S, Zheng L, Shen B, Tao Y (2016) Shade avoidance 6 encodes an Arabidopsis flap endonuclease required for maintenance of genome integrity and development. Nucleic Acids Res **44:** 1271–1284

Zheng Z, Guo Y, Novák O, Chen W, Ljung K, Noel JP, Chory J (2016) Local auxin metabolism regulates environment-induced hypocotyl elongation. Nat Plants **2:** 16025

Zourelidou M, Absmanner B, Weller B, Barbosa IC, Willige BC, Fastner A, Streit V, Port SA, Colcombet J, de la Fuente van Bentem S, et al (2014) Auxin efflux by PIN-FORMED proteins is activated by two different protein kinases, D6 PROTEIN KINASE and PINOID. eLife **3:** e02860

Zourelidou M, Müller I, Willige BC, Nill C, Jikumaru Y, Li H, Schwechheimer C (2009) The polarly localized D6 PROTEIN KINASE is required for efficient auxin transport in Arabidopsis thaliana. Development **136:** 627–636

SHADE AVOIDANCE 4 is Required for Proper Auxin Distribution in the *Arabidopsis* Hypocotyl

Yanhua Ge, Fenglian Yan, Melina Zourelidou, Meiling Wang, Karin Ljung, Astrid Fastner, Ulrich Z. Hammes, Martin Di Donato, Markus Geisler, Claus Schwechheimer, Yi Tao

Supplemental Experimental Methods

Quantification of Free IAA

For quantification of free IAA, Col-0, *sav4* and *sav3-1* mutant seedlings were grown in white light for six days and then treated with or without simulated shade for one hour. The aerial parts of the seedlings were collected in three replicates (around 15 mg tissue/sample). Sample purification and IAA quantification using GC-MS/MS (gas-chromatography-tandem mass spectrometry) were performed as described (Andersen et al., 2008).

Acropetal Auxin Transport

Acropetal hypocotyl auxin transport was measured according to Lewis and Muday (Lewis and Muday, 2009). Radioactive auxin was applied as agar droplet to each 10 apical (cut) hypocotyls of low light-grown seedlings (10 µmol m^{-2} s^{-2}, 5 dag) and cut hypocotyl segments were counted after 3h. Means of wild-type hypocotyls (n = 4 with 3-times 10 hypocotyls) was set as 100%.

Oocyte Auxin Efflux Essays

Xenopus laevis oocyte preparation was based on a method described previously (Broer, 2010) and the oocyte auxin efflux assays were performed according to a recent publication (Zourelidou et al., 2014), except that 75 ng/µL cRNA of *SAV4* were injected either alone or with 150 ng/µL *PIN3* cRNA and/or

D6PK cRNA for analysis.

PIN3 Immunoblotting

Membrane protein extracts were prepared as published (Willige et al., 2013). Four-day-old etiolated seedlings were frozen in liquid nitrogen and homogenized in extraction buffer (50 mM Tris-HCl pH 7.5, 150 mM NaCl, 0.1 mM MG132, 1 mM PMSF, complete EDTA-free protease inhibitor [Roche, Penzberg, Germany], and PhosStop phosphatase inhibitor cocktail [Roche, Penzberg, Germany]). After homogenization, extracts were centrifuged for 10 min at 10,000 X *g*, and the supernatants were further centrifuged for 1 hour at 100,000 X *g* in a MTX500 micro centrifuge (ThermoScientific). The resulting pellet was re-suspended in 2 X Laemmli buffer and heated by 45°C for 5 min. The equivalent of 20 µg total proteins was separated on 10% SDS-PAGE gels and transferred to nitrocellulose. The blots were probed with anti-PIN3 (1: 2000, Nottingham Arabidopsis Stock Centre) and secondary anti-goat antibody (1: 8000, A5420 Sigma). Coomassie Brilliant Blue staining was used to control for equal loading.

PIN3 Phosphorylation Experiment

In vitro phosphorylation experiments were carried out using purified recombinant GST-D6PK and GST-PIN3HL in combination with purified recombinant His-SAV4 proteins (Zourelidou et al., 2014). The recombinant proteins were added to the kinase reaction mix, containing 25 mM Tris-HCl pH 7.5, 5 mM $MgCl_2$, 0.2 mM EDTA, 1 X Complete protease inhibitor cocktail (Roche), and 0.5 µCi ^{32}P- ATP (370 MBq, specific activity 185 TBq; Hartmann Analytic). Reactions were incubated at 28 °C for 1 hour and stopped by addition of 5 X Laemmi buffer and boiled for 5 min. Reactions were subsequently separated over 10% acrylamide gels, coomassie stained and dried. Phosphorylation was

detected by autoradiography and protein loading was controlled by commassie staining.

Supplemental References

Andersen SU, Buechel S, Zhao Z, Ljung K, Novak O, Busch W, Schuster C, Lohmann JU (2008) Requirement of B2-type cyclin-dependent kinases for meristem integrity in Arabidopsis thaliana. Plant Cell **20:** 88-100

Broer S (2010) Xenopus laevis Oocytes. Methods Mol Biol **637:** 295-310

Lewis DR, Muday GK (2009) Measurement of auxin transport in Arabidopsis thaliana. Nature Protocols **4:** 437-451

Willige BC, Ahlers S, Zourelidou M, Barbosa IC, Demarsy E, Trevisan M, Davis PA, Roelfsema MR, Hangarter R, Fankhauser C, Schwechheimer C (2013) D6PK AGCVIII kinases are required for auxin transport and phototropic hypocotyl bending in Arabidopsis. Plant Cell **25:** 1674-1688

Zourelidou M, Absmanner B, Weller B, Barbosa IC, Willige BC, Fastner A, Streit V, Port SA, Colcombet J, de la Fuente van Bentem S, Hirt H, Kuster B, Schulze WX, Hammes UZ, Schwechheimer C (2014) Auxin efflux by PIN-FORMED proteins is activated by two different protein kinases, D6 PROTEIN KINASE and PINOID. Elife **3**

Supplemental Figures

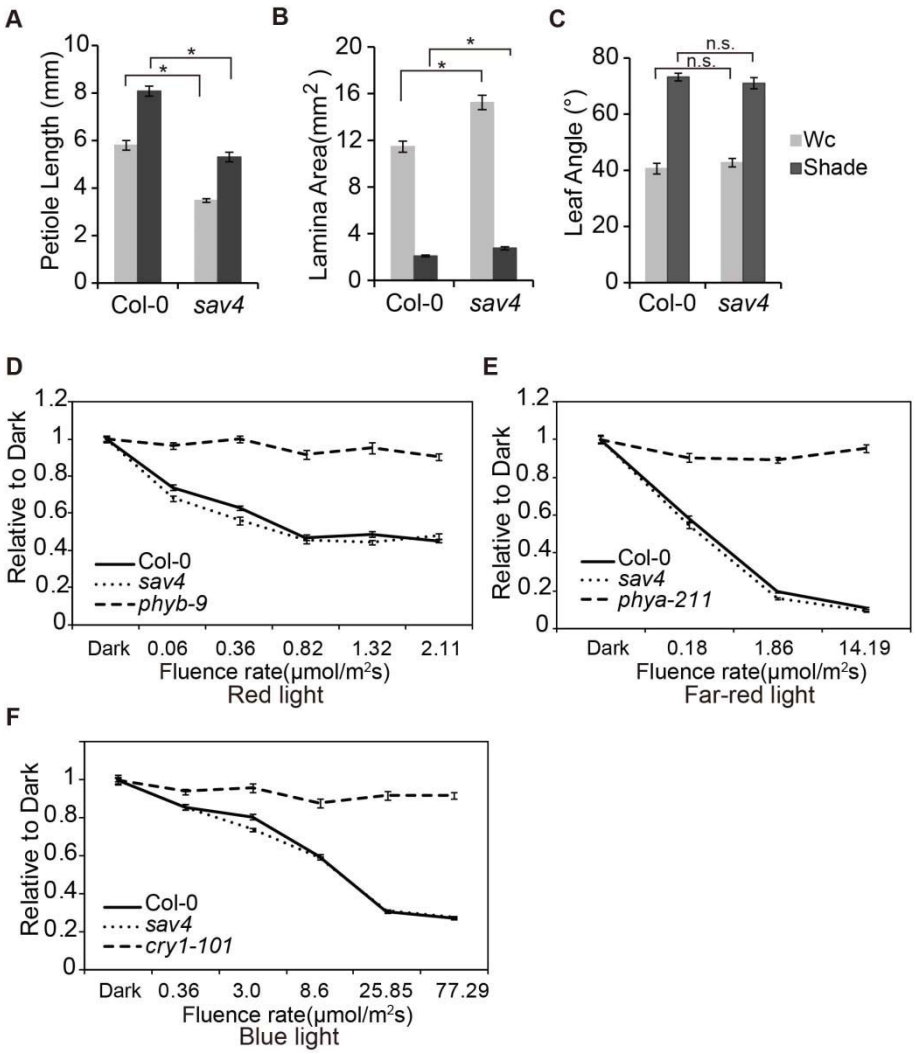

Supplemental figure 1. Phenotypes of *sav4*. (A-B) Petiole length (A) and lamina size (B) of the *sav4* mutant. Six-day-old seedlings were left in Wc or transferred to shade for three weeks. Petiole length and lamina area of the first set of true leaves were measured. (C) Leaf hyponasty phenotype of the *sav4* mutant. Six-day-old seedlings were left in Wc or transferred to shade for three days. Angles between the cotyledon petiole and an artificial horizontal line drawn perpendicular to the hypocotyl were measured. (D-F) Fluence-rate responses to continuous red light (D); far-red light (E) and blue light (F). Error bars represent the SEM (n ≥ 20). Student's *t* test, compared with the wild type: * P < 0.01 and not significant (n.s.) with P > 0.05.

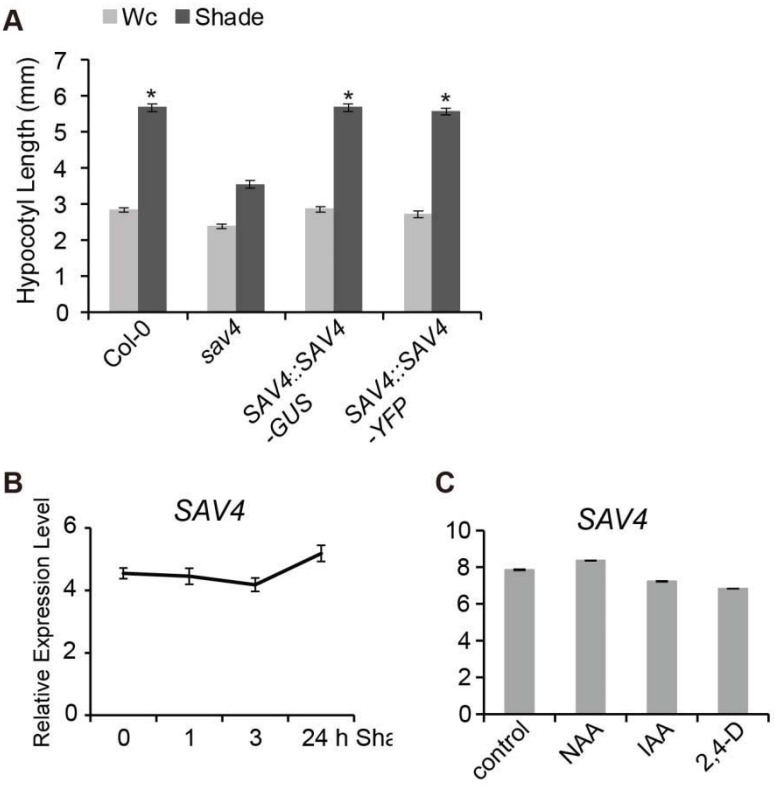

Supplemental figure 2. Expression analysis of *SAV4.* (A) Complementation of the mutant hypocotyl phenotype by the wild-type genomic *SAV4* sequence fused with GUS (*SAV4::SAV4-GUS*) or YFP (*SAV4::SAV4-YFP*). Error bars represent the SEM (n ≥ 20). Student's *t* test, compared with *sav4*: *P < 0.01. (B) Quantification of the transcript levels of *SAV4*. Six-day-old light-grown wild type seedlings were treated with shade and relative expression levels of *SAV4* were measured using qRT-PCR and were normalized to the reference gene. Error bars represent the SEM (n = 3). (C) Relative expression level of *SAV4* in response to exogenous auxin treatments. Six-day-old light-grown wild type seedlings were treated for 3 h with 10 µM naphthylacetic acid (NAA), 10 µM indole-3-acetic acid (IAA) or 1 µM 2,4-dichlorophenoxyacetic acid (2,4-D). Error bars represent the SEM (n = 3).

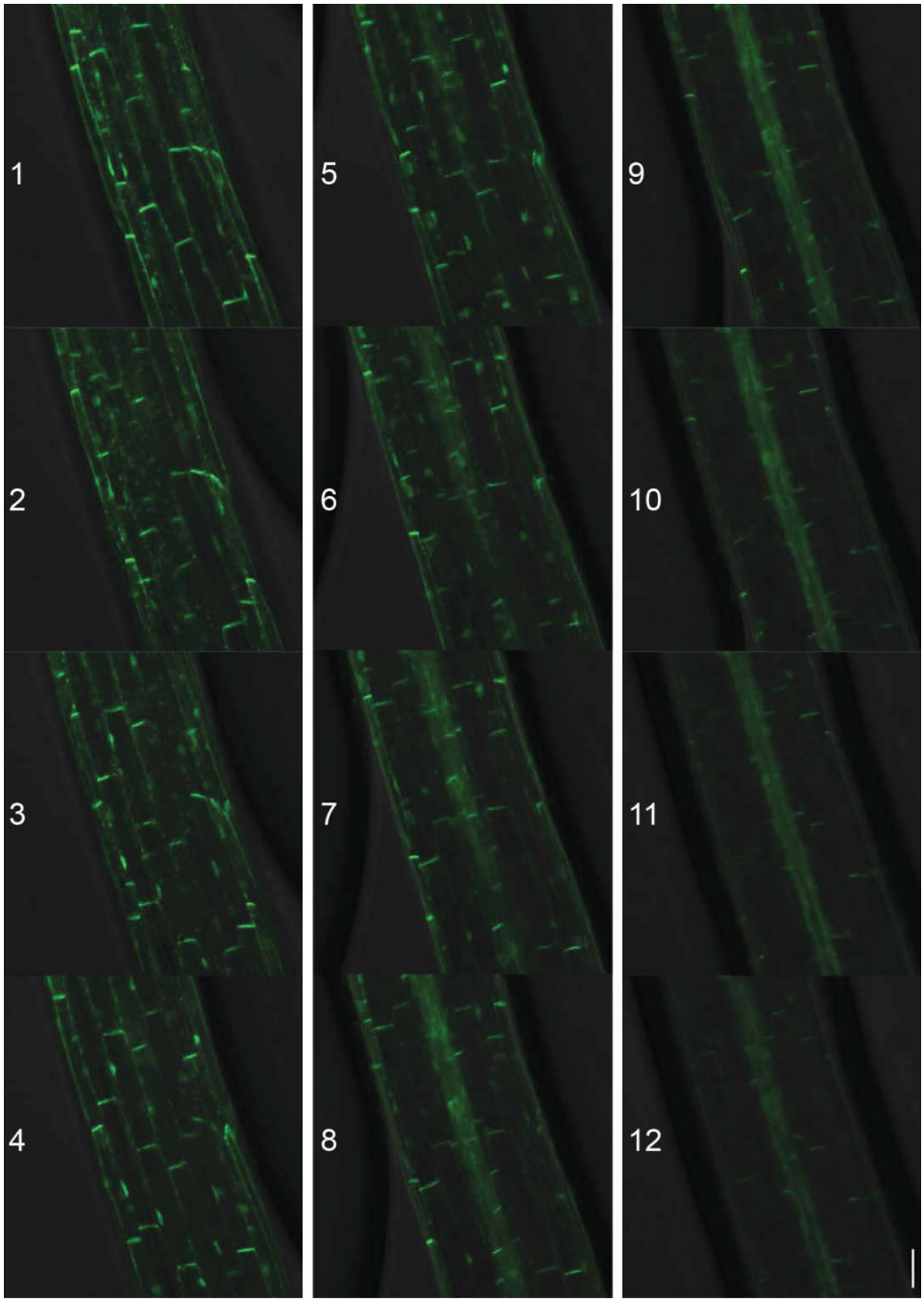

Supplemental figure 3. Z-stacks of hypocotyls of *SAV4::SAV4-YFP* from epidermis into vasculature. Scale bar = 50 µm.

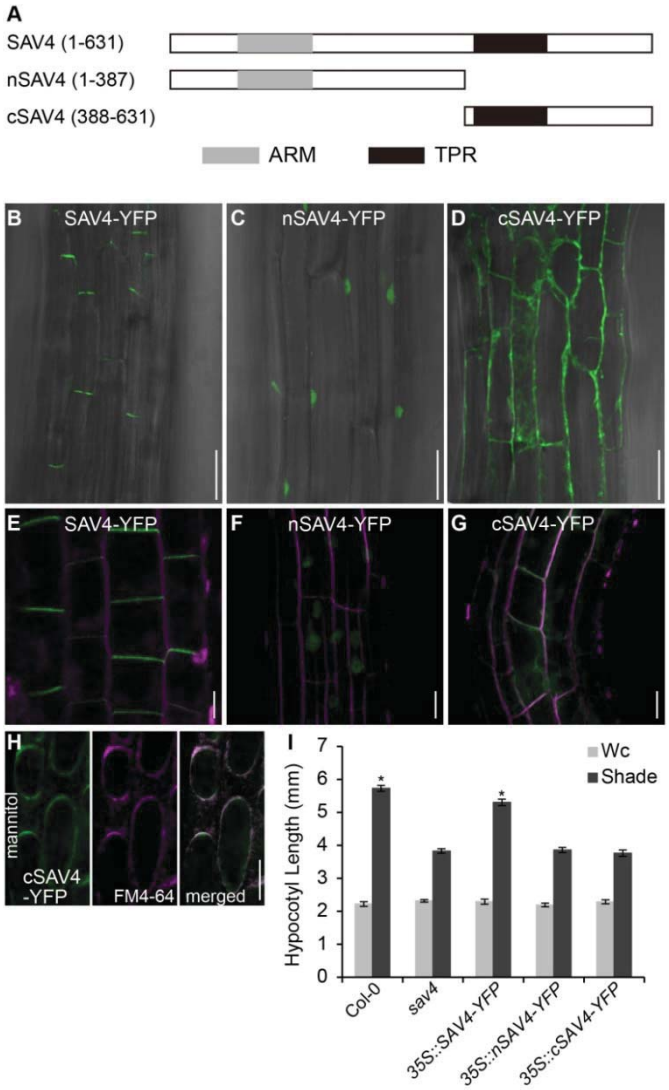

Supplemental figure 4. Specific domains of SAV4 determine its localization and function. (A) Diagram of full-length and truncated SAV4 used in localization and rescue experiments. Grey and black boxes represent ARM repeat- and TPR-like domains, respectively. Numbers indicate amino acids included in the fragment. (B-G) Subcellular localization of *35S::SAV4-YFP*, *35S::nSAV4-YFP* and *35S::cSAV4-YFP* in the hypocotyl epidermis (B-D) and in the root epidermal cells (E-G). Green and magenta fluorescence represent the signals of YFP and FM4-64 respectively. (H) Plasmolysis experiment showing that some of cSAV4-YFP protein still localizes to the plasma membrane. Scale bar = 50 µm (B-D),10 µm (E-H). (I) Quantification of the hypocotyl length of the transgenic seedlings used in (B-G). Error bars represent the SEM (n ≥ 20). Student's *t* test, compared with *sav4*: *P < 0.01.

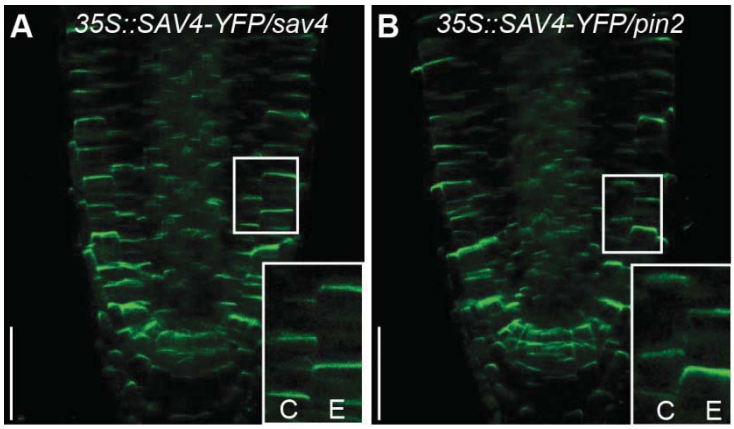

Supplemental figure 5. Polar targeting of SAV4 is unaltered in *pin2* mutant. (A-B) Representative confocal images of five-day-old *35S::SAV4-YFP* transgenic seedlings in *sav4* (A) and *pin2* (B) mutant background. E, epidermal cell files; C, cortical cell files. Scale bar = 50 µm.

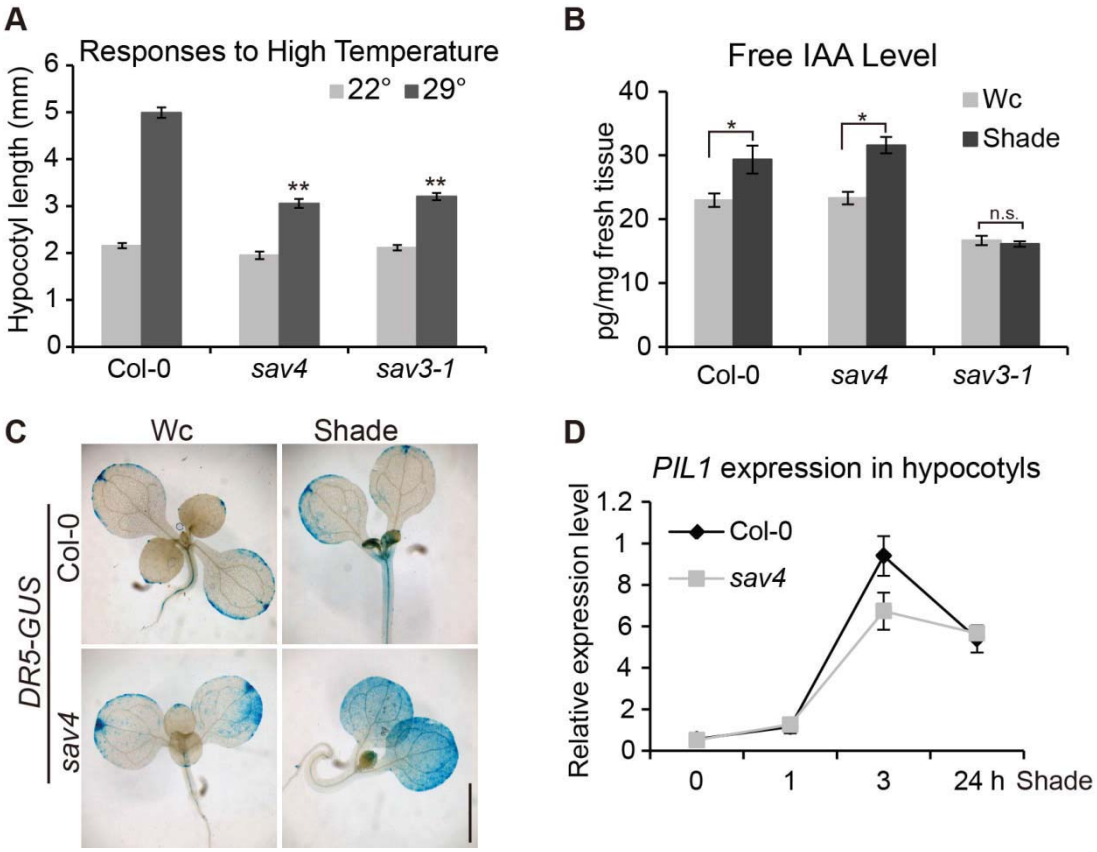

Supplemental figure 6. *sav4* is normal in auxin biosynthesis. (A) Responses of *sav4* to the high temperature (n ≥ 20). (B) Free IAA levels in Col-0, *sav4* and *sav3-1* mutants under white light and simulated shade. Seedlings were grown in white light and moved to white light or shade for one hour. The aerial parts were harvested to measure free IAA level (n = 3). (C) Expression of the *DR5::GUS* reporter in Col-0 and *sav4* background upon shade treatment. Six-day-old seedlings were left in Wc or transferred to shade for one day. Scale bar = 1 mm. (D) Quantification of the auxin-independent and shade-induced gene, *PIL1*, in hypocotyls. Relative expression level as compared to a reference gene (At1G13320) is shown (n = 3). Error bars represent the SEM. Student's *t* test: ** P < 0.01, * P < 0.05 and not significant (n.s.) with P > 0.05.

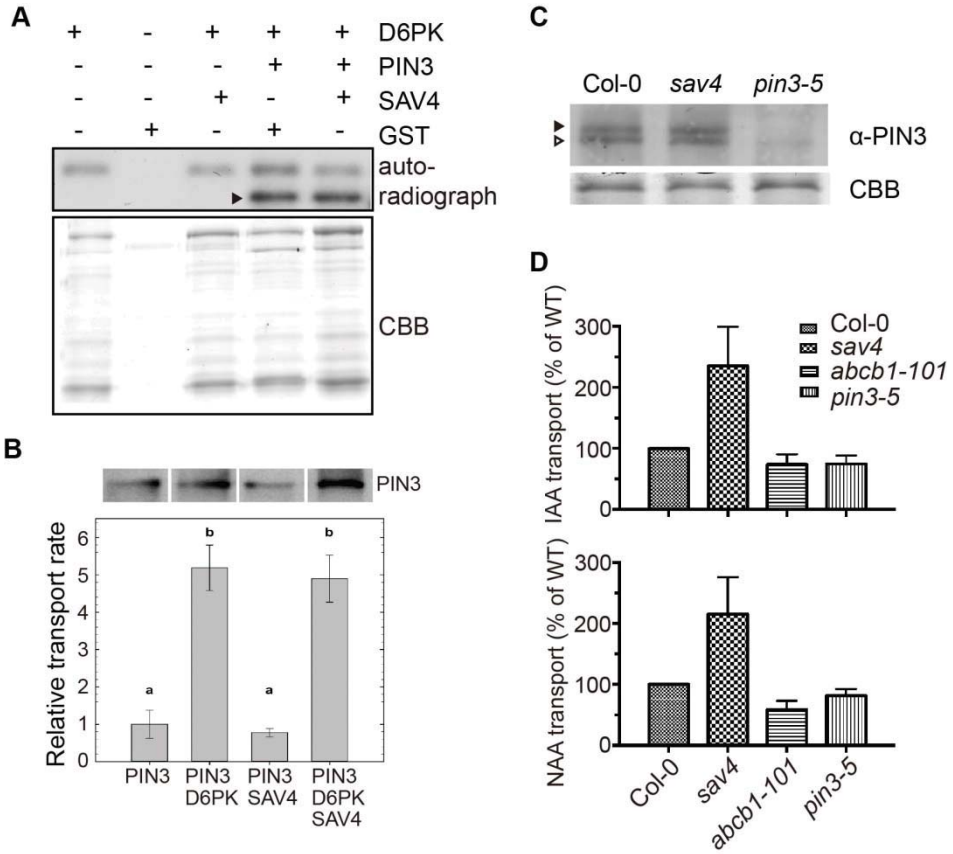

Supplemental figure 7. SAV4 is not directly involved in D6PK-activated PIN3-mediated auxin efflux. (A) Recombinant GST-D6PK phosphorylated the hydrophilic loop of PIN3, but not recombinant HIS-SAV4. SAV4 exerted no effect on the phosphorylation of PIN3 by D6PK *in vitro*. Arrowhead indicates the phosphorylated PIN3. (B) Results of the auxin efflux assays conducted in Xenopus oocytes expressing PIN3, D6PK and SAV4. The upper panel shows anti-PIN3 immunoblot of microsomal membrane of the corresponding oocytes used in the auxin efflux assay. The averages of four biological replicates are shown after normalization to the mock control. ANOVA and Holm-Sidak *post hoc*Test: b = $p < 0.001$. (C) Immunoblot with an anti-PIN3 antibody of membrane protein extracts from four-day-old etiolated seedlings. Black and empty triangles represent phosphorylatedand and unphosphorylated PIN3, respectively. CBB, Coomassie Brilliant Blue-stained gel, loading control. (D) Acropetal auxin transport activity in hypocotyls of light-grown seedlings. The mutation in *SAV4* significantly increased the acropetal transport of IAA and NAA. Values shown are means of at least three independent experiments ± SD (standard deviation).

160 **Supplemental Table 1.** Primers used in this study.

Purpose	Name	Sequence
SAV4::SAV4 cloning	SAV4-LP	TATGACCATGATTACTGAGGCTTATTTGCTTAA
	SAV4-RP	TGCAGGTCGACTCTACCTAATACTAACTTACAA
SAV4::SAV4-GUS cloning	SAV4-3'UTR-LP1	GGAGGCAAACAATGAAACCTTGAAACACAACA
	SAV4-3'UTR-RP	ACGACGGCCAGTGCCCCTAATACTAACTTACA
	SAV4-LP	TATGACCATGATTACTGAGGCTTATTTGCTTAA
	SAV4-GUS-RP	TACAGGACGTAACATTATTTCATCTTCTGCA
SAV4::SAV4-YFP cloning	SAV4-3'UTR-LP2	GAGCTGTACAAGTAAAACCTTGAAACACAACA
	SAV4-3'UTR-RP	ACGACGGCCAGTGCCCCTAATACTAACTTACA
	SAV4-LP	TATGACCATGATTACTGAGGCTTATTTGCTTAA
	SAV4-YFP-RP	GCCCTTGCTCACCATTATTTCATCTTCTGCA
35S::SAV4-YFP cloning	SAV4-YFP-LP	GAGCTCGGTACCCGGATGGATAAAGCTTCCT
	SAV4-YFP-RP	GCCCTTGCTCACCATTATTTCATCTTCTGCA
35S::nSAV4-YFP cloning	SAV4-YFP-LP	GAGCTCGGTACCCGGATGGATAAAGCTTCCT
	nSAV4-YFP-RP	GCCCTTGCTCACCATAGGCATACTCTTCTCC
35S::cSAV4-YFP cloning	cSAV4-YFP-LP	GAGCTCGGTACCCGGATGAAAGAGGACCTTC
	SAV4-YFP-RP	GCCCTTGCTCACCATTATTTCATCTTCTGCA
His-SAV4 cloning	PET28a-SAV4-LP	ATGGGTCGCGGATCCATGGATAAAGCTTCCTC
	PET28a-SAV4-RP	GCGGCCGCAAGCTTGTCATATTTCATCTTCTGC
sav4 genotyping	SAV4-CAPS-LP	GGAGTCGAGAAAAGCCGAGGAATG
	SAV4-CAPS-RP	CTGGAAGATTCACCAAGAACTCAGG
abcb1 genotyping	ABCB1-LP	CTCCGAGTTAAATGCAGCAAC
	ABCB1-RP	GAAAAGCTGACCTTGTTGCTG
abcb19 genotyping	ABCB19-LP	GCAATTGCAATTCTCTGCTTC
	ABCB19-RP	CTCAGGCAATTGCTCAAGTTC

	LBb 1.3	ATTTTGCCGATTTCGGAAC
qRT-PCR		
IAA19 (At3g15540)	Q-IAA19-LP	GGGTTAGGGTATGTGAAAGTGAGC
	Q-IAA19-RP	CGTATTCGCAGTTGTCACCATC
PIL1 (At2g46970)	Q-PIL1-LP	TACAAGGATGATAAGGCTTCATTGTTGG
	Q-PIL1-RP	CGGACGCAGACTTTGGGAATTG
PIN3 (At1g70940)	Q-PIN3-LP	GCGTCAATAAAAACCCGAAA
	Q-PIN3-RP	GGCGTCTTTTGGTCTCTCTG
REF3 (At1g13320)	Q-REF3-LP	GGAGCCAACTAGGACGGATCTGG
	Q-REF3-RP	GTAGATCAATCCCAATAACCTGGTTCACTT
SAV4 (At5g10200)	Q-SAV4-LP	GACAGAGACTGAAATGGGAGAAGAG
	Q- SAV4-RP	GTTGTAGCAAGAGATGACACTGAGC

161